IEEE Access
Multidisciplinary | Rapid Review | Open Access Journal

Received March 14, 2019, accepted April 26, 2019, date of publication April 30, 2019, date of current version May 13, 2019.

Digital Object Identifier 10.1109/ACCESS.2019.2914020

Transceiver Optimization for DF MIMO Relay Systems With a Wireless Powered Relay Node

BIN LI[1], (Senior Member, IEEE), HANYU CAO[1], YUE RONG[2], (Senior Member, IEEE), TONGHUA SU[3], GANG YANG[4], (Member, IEEE), AND ZHIQIANG HE[5], (Member, IEEE)

[1]School of Electrical Engineering and Information, Sichuan University, Chengdu 610065, China
[2]School of Electrical Engineering, Computing and Mathematical Sciences, Curtin University, Perth, WA 6845, Australia
[3]School of Software, Harbin Institute of Technology, Harbin 150001, China
[4]The National Key Laboratory of Science and Technology on Communications, and the Center for Intelligent Networking and Communications, University of Electronic Science and Technology of China, Chengdu 611731, China
[5]Key Laboratory of Universal Wireless Communication, Ministry of Education, Beijing University of Posts and Telecommunications, Beijing 100876, China

Corresponding author: Yue Rong (y.rong@curtin.edu.au)

This work was supported in part by the National Natural Science Foundation of China under Grant 61701124 and Grant 61601100, in part by the grant from the Science and Technology on Space Intelligent Control Laboratory under Grant KGJZDSYS-2018-03, in part by the grant from Sichuan Science and Technology Program under Grant 2019YJ0105, and in part by the grant from Fundamental Research Funds for the Central Universities (China).

ABSTRACT In this paper, a two-hop decode-and-forward (DF) multiple-input multiple-output (MIMO) relay system is investigated, where the relay node harvests the radio frequency energy transmitted by the source node and uses the harvested energy to forward information from source to destination. We consider both the time switching (TS) and power splitting (PS)-based protocols between wireless information and energy transfer. For each protocol, we study the optimal source and relay covariance matrices to maximize the source-destination mutual information (MI), under the source energy constraint and the harvested energy constraint at the relay node. For the TS protocol, the peak transmission power constraints are also considered at the source and relay nodes. The numerical results are presented to demonstrate the effectiveness of the proposed methods. It is shown that the proposed DF relay system achieves a higher MI than that of the amplify-and-forward relay system. Moreover, the PS-based protocol achieves a higher system MI than the TS-based protocol, but at a higher computational complexity.

INDEX TERMS Decode-and-forward, energy harvesting, MIMO relay, power splitting, time switching.

I. INTRODUCTION

A. BACKGROUND

The number of Internet of Things (IoT) devices has increased dramatically in recent years. A significant challenge for these IoT devices is their energy and lifetime constraints as they are powered by batteries in many applications [1]. The life time of IoT devices can be extended through battery replacing, which can be costly. Moreover, battery replacing cannot be easily performed in many cases because of economic or physical constraints. For instance, in some applications the devices may be embedded inside human bodies or building structures.

Thus, energy harvesting (EH) techniques are important for IoT systems, where energy is harvested from external sources [1]. Traditional EH technologies, which rely mainly on natural energy resources (e.g. wind and solar energy), have constraints in that these energy sources are intermittent and hence difficult to control. Therefore, they cannot provide reliable power supply to IoT devices. To overcome the constraints of traditional EH technologies, a new technique using radio frequency (RF) signals for energy transfer has been developed [2], [3]. Compared to traditional EH techniques, the RF-based wireless powered communication (WPC) technique provides great convenience to IoT systems.

B. LITERATURE REVIEW

In [4], an ideal receiver capable of simultaneous EH and information decoding (ID) has been proposed, and a capacity-energy function has been introduced to characterize the trade-off between the achievable information rate and the harvested energy. However, for practical implementation, such ideal receiver has two challenges [2]. Firstly, circuits designed for energy harvesting usually cannot decode the information

The associate editor coordinating the review of this manuscript and approving it for publication was Emanuele Lattanzi.

carried in the signal. To coordinate wireless energy transfer (WET) and wireless information transfer (WIT), power splitting (PS) and time switching (TS) protocols have been developed in [5]. Secondly, as WET and WIT systems work at different sensitivity (−10 dBm for EH receivers and -60 dBm for ID receivers), the design of conventional ID receivers may be suboptimal for an EH receiver. To solve this issue, integrated and separated architecture receivers have been proposed in [2] for a more general dynamic PS protocol, which includes the PS and TS protocols as special cases. Waveform optimization for efficient WET has been investigated in [6] and [7].

Through installing multiple antennas at the access point of IoT networks, RF energy can be more efficiently delivered to IoT devices compared to single-antenna systems [8]. A multiple-input multiple-output (MIMO) broadcasting system using a separated architecture EH and ID receiver has been studied in [5], where the rate-energy regions have been established for the PS and TS protocols. A multiple-input single-output (MISO) system has been studied in [9], where joint optimization of the PS ratio and the transmit beamforming vector is performed to minimize the total transmission power under signal-to-interference-plus-noise ratio (SINR) constraints. Wireless powered multi-user systems with massive antennas at the base station have been studied in [10] and [11].

Relay technology can be applied to expand the coverage of wireless systems. Using the WPC technology, relay nodes are capable of harvesting RF energy and receiving information from the source node. Then, by using the harvested energy, relay nodes forward the received information to the destination node. The application of relays in WPC has been investigated in [12]–[30]. TS and PS based relay protocols for WPC have been investigated in [12] for an amplify-and-forward (AF) relay network. In [13], a cooperative network has been studied, where multiple source-destination pairs communicate simultaneously under the aid of an EH relay node. The impact of the user energy distribution on the system performance has been investigated in [13]. WPC using randomly located decode-and-forward (DF) relay nodes has been investigated in [14], where it has been demonstrated that the same diversity gain as conventional self-powered relays is achievable through using EH relays. A game theory based distributed PS framework has been proposed in [15] for WPC in interference relay systems. In [16], WPC in a relay system using the orthogonal frequency-division multiplexing technology has been investigated. WPC for cooperative communication systems using the PS protocol has been investigated in [17], where the optimal power allocation and PS ratio are studied.

The application of WPC in MIMO relay systems has been investigated in [18]–[30]. Performance trade-offs of applying EH in MIMO relay systems have been investigated in [18] under several receiver architectures. Challenges in this research topic have also been presented in [18]. A space-time block code based AF MIMO relay system with a multi-antenna EH receiver has been studied in [19] and [20], where joint source and relay precoding matrices design has been considered to achieve trade-offs between the information rate and the energy transfer capability. In [21], WPC in massive MIMO relay systems has been studied. The benefit of massive antennas in wireless power transfer based two-way relaying has been illustrated in [22]. WPC using full duplex MIMO relays has been discussed in [23]–[25]. Recently, WPC in AF MIMO relay systems with EH relay nodes has been investigated in [26]–[30], where joint source and relay matrices design has been investigated to maximize the system rate.

C. CONTRIBUTIONS

We investigate a dual-hop DF MIMO relay system, where an EH receiver is installed at the relay node to enable the energy and information transfer. A relay node is particularly beneficial in scenarios where the direct link is much weaker compared with the link via the relay node, because of path attenuation and shadowing by obstacles. The practical TS based protocol and the PS based protocol are adopted during the first phase. Then, during the second phase, the relay node decodes the received information and re-encodes it into new signals, and then uses the harvested energy to forward these signals to the destination node.

The main contributions of this paper compared with [18]–[30] are listed below.

(1) For the TS based protocol, a more general source node energy constraint is proposed which enables the source node to operate flexibly at various power levels adaptive to WET at the first interval and WIT at the second interval.

(2) We investigate the joint optimization of the TS factor and the source and relay covariance matrices to maximize the source-destination system mutual information (MI) under the proposed source energy constraint and the harvested energy constraint at the relay node. We derive the optimal structure of the source and relay matrices, which reduces the original problem to a simpler power allocation problem.

(3) We show that the achievable system MI is a unimodal function of the TS factor. Based on this fact, a two-step approach is proposed to solve the power allocation problem efficiently. In particular, the optimal TS factor is obtained by a golden section search [31]. For a given TS factor, the optimization problem is convex and can be solved based on the first order optimality condition.

(4) For practical applications, peak power constraints are considered at both the source node and the relay node. We propose a decomposition based algorithm to solve the optimization problem based on the solution of the power allocation problem without peak transmission power constraints. This algorithm reduces the problem into simpler subproblems which can be efficiently solved by the water-filling algorithm.

(5) For the PS based protocol, we investigate the joint optimization of the PS vector and the source and relay covariance matrices to maximize the system MI, subjecting to the energy constraints at the source and relay nodes. We show that the

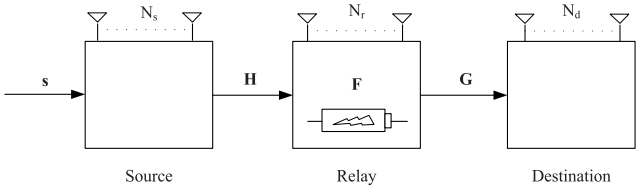

FIGURE 1. A dual-hop DF MIMO relay system with an EH relay node.

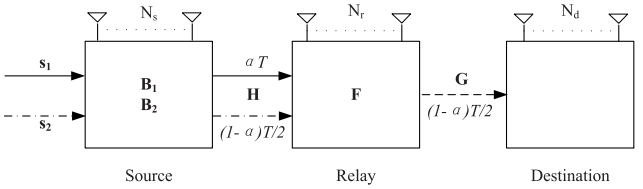

FIGURE 2. The system with the TS based protocol.

optimization problem can be recast to a convex optimization problem, and propose an algorithm to solve this problem efficiently based on the primal-dual interior point method. For this purpose, the corresponding Newton search direction of the primal and dual variables is derived.

(6) It is shown that the proposed wireless powered DF relay system has a higher MI than a wireless powered AF relay system. Moreover, the PS based protocol achieves a higher system MI than the TS based protocol (both with and without peak power constraints), but at a higher computational complexity. This performance-complexity trade-off is interesting for system designers.

One example of practical applications of the system and algorithms proposed in this paper is a heterogeneous network consisting of devices with different capabilities, where inactive devices with MIMO capabilities can be exploited as relays to assist active users in the network [18]. Moreover, through harvesting the RF energy transferred from the source node, the relay node does not need to spend its own energy to forward information from source to destination. This helps to provide motivation for a selfish node to participate in the relay scheme.

D. STRUCTURE

The rest of this paper is organized as follows. The model of a dual-hop wireless powered DF MIMO relay system is presented in Section II. The transceiver optimization problems for the TS and PS based protocols are also formulated in this section. The proposed algorithms for the TS based protocol are developed in Section III. In Section IV, we present the proposed algorithm for the PS based protocol. Numerical examples are shown in Section V to demonstrate the performance of the proposed algorithms. Finally, we conclude our paper in Section VI.

II. SYSTEM MODEL AND PROBLEM FORMULATIONS

We consider a two-hop three-node MIMO relay system where the source node communicate with the destination node with the aid of a relay node as shown in Fig. 1. The source, relay, and destination nodes are installed with N_s, N_r, and N_d antennas, respectively, to obtain the benefits of the MIMO technology. We assume that the source and destination nodes have their own power supply, but the relay node relies on harvesting the RF energy transferred by the source node. The harvested energy is stored in a battery, which then supplies power for the relay node to forward the signals. The DF relay strategy is chosen, as in an AF relay, the noise at the relay node is amplified and forwarded to the destination node, while a DF relay stops such noise propagation.

The system completes one source-destination communication cycle in two phases. During the first phase, signals carrying energy and information are sent from the source to the relay node. During the second phase, information-carrying signals received by the relay are decoded, re-encoded, and forwarded to the destination. Similar to [19], [20], [26], [30], the direct source-destination link is not considered, as compared to the link via the relay node, path attenuation and shadowing effects are much more severe on the direct link. This is a typical scenario where relay nodes are useful. If there exists a strong direct link, it is better to have a one-hop source-relay communication through the direct path.

In this paper, two practical protocols – the time switching protocol and the power splitting protocol [5] are adopted for the energy and information transmission at the first phase.

A. THE TS BASED PROTOCOL

For the TS protocol, as shown in Fig. 2, we divide the total time T of one communication cycle into three intervals. During the first time interval of αT, RF energy is transferred from the source to the relay node, where $0 < \alpha < 1$ is the time switching factor. During the following time interval of $(1-\alpha)T/2$, information signals are sent from the source node to the relay node. During the last time interval of $(1-\alpha)T/2$, the relay node forwards the information signals to the destination node.[1] For the sake of notational simplicity, hereafter we set $T = 1$.

During the first time interval, the transmitted RF-band signal at the ith antenna of the source node is given by $x_i(t) = \sqrt{2}\mathrm{Re}\{s_i(t)e^{j2\pi ft}\}$, $i = 1, \ldots, N_s$, where $\mathrm{Re}\{\cdot\}$ stands for the real part of a complex number, f is the carrier frequency, and $s_i(t)$ is the complex baseband signal with $E\{s_i(t)s_j^\star(t)\} = b_{1,i,j}$. Here $E\{\cdot\}$ stands for the statistical expectation, $(\cdot)^\star$ denotes the complex conjugate, and $b_{1,i,j}$ is the (i,j)th element of $\boldsymbol{B}_1$. Thus, the power of the transmitted signals is constant as long as $b_{1,i,j}$ are fixed. By introducing $\boldsymbol{s}_1 = [s_{1,1}(t), \ldots, s_{1,N_s}(t)]^T$, we have $E\{\boldsymbol{s}_1\boldsymbol{s}_1^H\} = \boldsymbol{B}_1$, where $(\cdot)^T$ and $(\cdot)^H$ denote transpose and Hermitian transpose, respectively. The received baseband signal vector at the relay node

[1] Note that the time allocated for the two intervals in information transmission can also be optimized to further increase the system MI. We found through numerical simulations that the performance gain is marginal. Moreover, adding an extra optimization variable increases the computational complexity. Considering the performance-complexity tradeoff, we decide to keep equal time allocation for the two intervals in information transmission.

is given by

$$\boldsymbol{y}_{r,1} = \boldsymbol{H}\boldsymbol{s}_1 + \boldsymbol{v}_{r,1} \tag{1}$$

where $\boldsymbol{H}$ is an $N_r \times N_s$ source-relay MIMO channel and $\boldsymbol{v}_{r,1}$ is the noise vector at the relay node at the first time interval. According to [5], [8]–[10], [26], the RF energy harvested by the relay node is proportional to the energy of the baseband received signal in (1), and is given by

$$E_r = \eta_1 \alpha \mathrm{tr}(\boldsymbol{H}\boldsymbol{B}_1\boldsymbol{H}^H) \tag{2}$$

where $0 < \eta_1 < 1$ is the energy conversion efficiency and $\mathrm{tr}(\cdot)$ denotes the matrix trace.[2]

During the second interval, an $N_s \times 1$ information-carrying signal vector $\boldsymbol{s}_2$ with $E\{\boldsymbol{s}_2\boldsymbol{s}_2^H\} = \boldsymbol{B}_2$ is transmitted to the relay node. The received signal vector at the relay node in the second interval is given by

$$\boldsymbol{y}_{r,2} = \boldsymbol{H}\boldsymbol{s}_2 + \boldsymbol{v}_{r,2} \tag{3}$$

where $\boldsymbol{y}_{r,2}$ and $\boldsymbol{v}_{r,2}$ are the received signal and the additive noise vectors at the relay node during the second interval, respectively. Then, the relay node decodes $\boldsymbol{y}_{r,2}$ and re-encodes the decoded information into an $N_r \times 1$ signal vector $\tilde{\boldsymbol{s}}_2$ with $E\{\tilde{\boldsymbol{s}}_2\tilde{\boldsymbol{s}}_2^H\} = \boldsymbol{F}$.

Finally, in the last interval, the relay node transmits $\tilde{\boldsymbol{s}}_2$ to the destination node. The received signal vector at the destination node can be written as

$$\boldsymbol{y}_d = \boldsymbol{G}\tilde{\boldsymbol{s}}_2 + \boldsymbol{v}_d \tag{4}$$

where $\boldsymbol{G}$ is an $N_d \times N_r$ MIMO channel matrix between the relay and destination nodes, $\boldsymbol{y}_d$ and $\boldsymbol{v}_d$ are the received signal and the additive noise vectors at the destination node, respectively.

We assume that $\boldsymbol{H}$ and $\boldsymbol{G}$ are quasi-static and known at the node responsible for the system optimization, which can be either the source or the destination node. Note that $\boldsymbol{H}$ and $\boldsymbol{G}$ can be estimated, for example, using approaches in [35] and the references therein. All noises are assumed to be zero-mean additive white Gaussian noise (AWGN). From (3) and (4), the MI between the source and destination nodes is the minimum of the MI of the source-relay link and that of the relay-destination link, which can be written as [36]

$$\mathrm{MI}(\alpha, \boldsymbol{B}_2, \boldsymbol{F}) = \frac{1-\alpha}{2} \min\{\log_2 |\boldsymbol{I}_{N_r} + \sigma_r^{-2}\boldsymbol{H}\boldsymbol{B}_2\boldsymbol{H}^H|, \log_2 |\boldsymbol{I}_{N_d} + \sigma_d^{-2}\boldsymbol{G}\boldsymbol{F}\boldsymbol{G}^H|\} \tag{5}$$

where $|\cdot|$ denotes the matrix determinant, $\boldsymbol{I}_n$ is an $n \times n$ identity matrix, σ_r^2 and σ_d^2 are the variances of the noise at the relay node and the destination node, respectively.

It can be seen that at the source node, the energy used to transmit $\boldsymbol{s}_1$ and $\boldsymbol{s}_2$ is $\alpha\mathrm{tr}(\boldsymbol{B}_1)$ and $\frac{1-\alpha}{2}\mathrm{tr}(\boldsymbol{B}_2)$, respectively. Since the source node is active for a duration of $\frac{1+\alpha}{2}$, the source node energy consumption constraint is given by

$$\alpha\mathrm{tr}(\boldsymbol{B}_1) + \frac{1-\alpha}{2}\mathrm{tr}(\boldsymbol{B}_2) \le \frac{1+\alpha}{2}P_s \tag{6}$$

where P_s is the nominal (average) source node power. We would like to note that the energy constraint (6) enables the source node to work flexibly at various power levels adaptive to WET at the first time interval and WIT at the second time interval, which is more flexible than a fixed power constraint at both intervals (i.e., $\mathrm{tr}(\boldsymbol{B}_1) \le P_s$ and $\mathrm{tr}(\boldsymbol{B}_2) \le P_s$).

The energy consumed by the relay node at the third interval to transmit $\tilde{\boldsymbol{s}}_2$ to the destination node can be written as

$$\frac{1-\alpha}{2}\mathrm{tr}(E\{\tilde{\boldsymbol{s}}_2\tilde{\boldsymbol{s}}_2^H\}) = \frac{1-\alpha}{2}\mathrm{tr}(\boldsymbol{F}). \tag{7}$$

In this paper, we consider that the circuit and signal processing energy consumed by the relay node consists of two parts [37]: A static part used for maintaining the basic circuit operations and a dynamic part depending on the amount of decode-and-forward processing at the relay node. In particular, taking into account multiple antennas [38], the static part is modeled as $\frac{1-\alpha}{2}N_rP_c$, where P_c is the per-antenna static power consumption. The dynamic part of the energy consumption is modeled as $\eta_2 E_r$, where $0 < \eta_2 < 1$. Based on (2) and (7), the relay node energy constraint is given by[3]

$$\frac{1-\alpha}{2}(\mathrm{tr}(\boldsymbol{F}) + N_rP_c) \le (1-\eta_2)E_r = \alpha\eta\mathrm{tr}(\boldsymbol{H}\boldsymbol{B}_1\boldsymbol{H}^H) \tag{8}$$

where $\eta = \eta_1(1-\eta_2)$.

When α approaches 0 or 1, the source and relay nodes transmission power may increase to a very large value, if only the energy constraints (6) and (8) are considered. To impose constraints on the peak power, we introduce

$$\mathrm{tr}(\boldsymbol{B}_1) \le P_{m,s},\ \mathrm{tr}(\boldsymbol{B}_2) \le P_{m,s},\ \mathrm{tr}(\boldsymbol{F}) \le P_{m,r} \tag{9}$$

where $P_{m,s}$ and $P_{m,r}$ are the peak power limits at the source node and the relay node, respectively ($P_{m,s} \ge P_s$ and $P_{m,r} \ge P_s$). From (5), (6), (8), and (9), for TS based wireless powered DF MIMO relay systems, the transceiver optimization problem which maximizes the source-destination MI subjecting to the energy and power constraints is given by

$$\max_{\alpha,\boldsymbol{B}_1,\boldsymbol{B}_2,\boldsymbol{F}} \ \mathrm{MI}(\alpha, \boldsymbol{B}_2, \boldsymbol{F}) \tag{10a}$$

$$\text{s.t. } \alpha\mathrm{tr}(\boldsymbol{B}_1) + \frac{1-\alpha}{2}\mathrm{tr}(\boldsymbol{B}_2) \le \frac{1+\alpha}{2}P_s \tag{10b}$$

$$\mathrm{tr}(\boldsymbol{F}) \le \min\left\{\frac{2\alpha\eta}{1-\alpha}\mathrm{tr}(\boldsymbol{H}\boldsymbol{B}_1\boldsymbol{H}^H) - N_rP_c, P_{m,r}\right\} \tag{10c}$$

$$\mathrm{tr}(\boldsymbol{B}_1) \le P_{m,s},\ \mathrm{tr}(\boldsymbol{B}_2) \le P_{m,s} \tag{10d}$$

$$0 < \alpha < 1, \quad \boldsymbol{B}_1 \ge 0, \quad \boldsymbol{B}_2 \ge 0, \quad \boldsymbol{F} \ge 0. \tag{10e}$$

[2] Extending the algorithms developed in this paper to wireless powered relay nodes where nonlinear energy harvesting models are adopted [7], [32]–[34] is an interesting future research topic.

[3] Similar to [5], [8]- [10], [26], it is assumed that all the energy harvested by the relay node in one communication cycle is consumed for relaying signals during this communication cycle. Energy accumulation and scheduling across multiple communication cycles is an interesting topic.

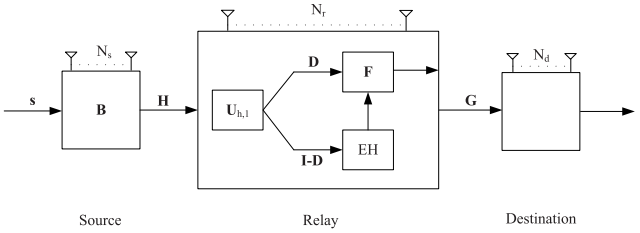

FIGURE 3. The system with a PS based energy-harvesting relay node.

B. THE PS BASED PROTOCOL

For the PS based protocol, one transmission cycle is divided into two equal time intervals. As shown in Fig. 3, during the first interval, an $N_s \times 1$ source signal vector $\boldsymbol{s}$ with $E\{\boldsymbol{s}\boldsymbol{s}^H\} = \boldsymbol{B}$ is transmitted to the relay node. The baseband received signal vector at the relay node is given by

$$\boldsymbol{y}_r = \boldsymbol{H}\boldsymbol{s} + \boldsymbol{v}_r \tag{11}$$

where $\boldsymbol{y}_r$ and $\boldsymbol{v}_r$ are the received signal and noise vectors at the relay node, respectively. During the second interval, the relay node multiplies $\boldsymbol{y}_r$ by $\boldsymbol{U}_h^H$ [26], where $\boldsymbol{H} = \boldsymbol{U}_h\boldsymbol{\Lambda}_h^{\frac{1}{2}}\boldsymbol{V}_h^H$ is the singular value decomposition (SVD) of $\boldsymbol{H}$ with the diagonal elements of $\boldsymbol{\Lambda}_h$ sorted in decreasing order. The dimensions of $\boldsymbol{U}_h$, $\boldsymbol{\Lambda}_h$, and $\boldsymbol{V}_h$ are $N_r \times R_h$, $R_h \times R_h$, and $N_s \times R_h$, respectively, where $R_h = \text{rank}(\boldsymbol{H})$ and rank$(\cdot)$ stands for the rank of a matrix. From (11), we have

$$\boldsymbol{z}_r = \boldsymbol{U}_h^H\boldsymbol{y}_r = \boldsymbol{\Lambda}_h^{\frac{1}{2}}\boldsymbol{V}_h^H\boldsymbol{s} + \boldsymbol{U}_h^H\boldsymbol{v}_r.$$

Using the PS protocol, the relay node then splits the signal vector $\bar{\boldsymbol{z}}_r \triangleq \boldsymbol{\Lambda}_h^{\frac{1}{2}}\boldsymbol{V}_h^H\boldsymbol{s}$ with a $R_h \times R_h$ PS matrix $\boldsymbol{D} = \text{diag}(d_1, \cdots, d_{R_h})$, where $\boldsymbol{D}^{\frac{1}{2}}\bar{\boldsymbol{z}}_r$ is used for information transmission and $(\boldsymbol{I}_{R_h} - \boldsymbol{D})^{\frac{1}{2}}\bar{\boldsymbol{z}}_r$ is reserved for energy harvesting. Here diag$(\cdot)$ stands for a diagonal matrix and $0 \le d_i \le 1$, $i = 1, \cdots, R_h$, is the PS ratio of the ith data stream. The harvested energy is stored in a battery, which then supplies power to $\boldsymbol{F}$ to forward the signals. Based on [5], the energy harvested at the relay node can be written as

$$\begin{aligned} E_r &= \frac{1}{2}\eta_1\, E\{\text{tr}((\boldsymbol{I}_{R_h} - \boldsymbol{D})^{\frac{1}{2}}\bar{\boldsymbol{z}}_r\bar{\boldsymbol{z}}_r^H(\boldsymbol{I}_{R_h} - \boldsymbol{D})^{\frac{1}{2}})\} \\ &= \frac{1}{2}\eta_1\text{tr}((\boldsymbol{I}_{R_h} - \boldsymbol{D})\tilde{\boldsymbol{B}}) \end{aligned} \tag{12}$$

where $\tilde{\boldsymbol{B}} \triangleq \boldsymbol{\Lambda}_h^{\frac{1}{2}}\boldsymbol{V}_h^H\boldsymbol{B}\boldsymbol{V}_h\boldsymbol{\Lambda}_h^{\frac{1}{2}}$.

Then, the relay node decodes $\boldsymbol{D}^{\frac{1}{2}}\bar{\boldsymbol{z}}_r$ and re-encodes the decoded information into an $N_r \times 1$ signal vector $\tilde{\boldsymbol{s}}$ with $E\{\tilde{\boldsymbol{s}}\tilde{\boldsymbol{s}}^H\} = \boldsymbol{F}_p$ and transmits $\tilde{\boldsymbol{s}}$ to the destination. The signal vector received at the destination is given by

$$\boldsymbol{y}_{d,p} = \boldsymbol{G}\tilde{\boldsymbol{s}} + \boldsymbol{v}_d. \tag{13}$$

From (11) and (13), the source-destination MI is given as [36]

$$\begin{aligned} \text{MI}(\boldsymbol{D}, \boldsymbol{B}, \boldsymbol{F}_p) = \frac{1}{2}\min\{&\log_2|\boldsymbol{I}_{R_h} + \sigma_r^{-2}\boldsymbol{D}^{\frac{1}{2}}\tilde{\boldsymbol{B}}\boldsymbol{D}^{\frac{1}{2}}|, \\ &\log_2|\boldsymbol{I}_{N_d} + \sigma_d^{-2}\boldsymbol{G}\boldsymbol{F}_p\boldsymbol{G}^H|\}. \end{aligned} \tag{14}$$

The energy consumed by the relay node to transmit $\tilde{\boldsymbol{s}}$ to the destination node is given by

$$\frac{1}{2}\text{tr}(E\{\tilde{\boldsymbol{s}}\tilde{\boldsymbol{s}}^H\}) = \frac{1}{2}\text{tr}(\boldsymbol{F}_p). \tag{15}$$

Based on (12) and (15) and considering the circuit and signal processing energy consumption, the relay node has the following energy constraint

$$\text{tr}(\boldsymbol{F}_p) \le \eta\text{tr}((\boldsymbol{I}_{R_h} - \boldsymbol{D})\tilde{\boldsymbol{B}}) - N_rP_c. \tag{16}$$

In addition, the energy constraint at the source node is given by

$$\text{tr}(\boldsymbol{B}) \le P_s. \tag{17}$$

From (14), (16), and (17), for a PS based wireless powered DF MIMO relay system, the transceiver optimization problem which maximizes the system MI subjecting to the energy and power constraints is given by

$$\max_{\boldsymbol{D},\boldsymbol{B},\boldsymbol{F}_p} \quad \text{MI}(\boldsymbol{D}, \boldsymbol{B}, \boldsymbol{F}_p) \tag{18a}$$

$$\text{s.t. } \text{tr}(\boldsymbol{B}) \le P_s \tag{18b}$$

$$\text{tr}(\boldsymbol{F}_p) \le \eta\text{tr}((\boldsymbol{I}_{R_h} - \boldsymbol{D})\tilde{\boldsymbol{B}}) - N_rP_c \tag{18c}$$

$$\boldsymbol{B} \ge 0, \quad \boldsymbol{F}_p \ge 0, \quad 0 \le d_i \le 1, \quad i = 1, \cdots, R_h. \tag{18d}$$

It will be shown later that as $\eta\text{tr}((\boldsymbol{I}_{R_h} - \boldsymbol{D})\tilde{\boldsymbol{B}}) < P_s$, there is no need to impose peak power constraint at the relay node as in the TS based protocol (9).

III. PROPOSED METHODS FOR THE TS BASED PROTOCOL

The problem (10) is nonconvex with matrix variables and is challenging to solve. In this section, we propose an efficient algorithm to solve the problem (10). Firstly, we derive the optimal structure of $\boldsymbol{B}_1$, $\boldsymbol{B}_2$, and $\boldsymbol{F}$, under which the problem (10) can be reduced to a simpler power allocation problem. Let us introduce $\boldsymbol{G} = \boldsymbol{U}_g\boldsymbol{\Lambda}_g^{\frac{1}{2}}\boldsymbol{V}_g^H$ as the SVD of $\boldsymbol{G}$ with the diagonal elements of $\boldsymbol{\Lambda}_g$ sorted in decreasing order. The dimensions of $\boldsymbol{U}_g$, $\boldsymbol{\Lambda}_g$, and $\boldsymbol{V}_g$ are $N_d \times R_g$, $R_g \times R_g$, and $N_r \times R_g$, respectively, where $R_g = \text{rank}(\boldsymbol{G})$.

Theorem 1: The optimal covariance matrices $\boldsymbol{B}_1$, $\boldsymbol{B}_2$, and $\boldsymbol{F}$ as the solution to the problem (10) has the following structure

$$\boldsymbol{B}_1^* = \lambda_b\boldsymbol{v}_{h,1}\boldsymbol{v}_{h,1}^H, \ \boldsymbol{B}_2^* = \boldsymbol{V}_h\boldsymbol{\Lambda}_2\boldsymbol{V}_h^H, \ \boldsymbol{F}^* = \boldsymbol{V}_g\boldsymbol{\Lambda}_f\boldsymbol{V}_g^H \tag{19}$$

where $(\cdot)^*$ denotes the optimal value, $\lambda_b > 0$, $\boldsymbol{v}_{h,1}$ is the first column of $\boldsymbol{V}_h$, $\boldsymbol{\Lambda}_2$ and $\boldsymbol{\Lambda}_f$ are $R_h \times R_h$ and $R_g \times R_g$ diagonal matrices, respectively.

Proof: See Appendix VI. ■

We can see from (19) that the optimal $\boldsymbol{B}_1$ is a rank-1 matrix which matches $\boldsymbol{v}_{h,1}$. This means that during the first interval, to maximize the energy harvested at the relay node, the source node transmission power should be transferred to the strongest subchannel of $\boldsymbol{H}$ [5], and the optimization of $\boldsymbol{B}_1$ boils down to that of λ_b (tr$(\boldsymbol{B}_1) = \lambda_b$). Moreover, the

optimal $\boldsymbol{B}_2$ and $\boldsymbol{F}$ match $\boldsymbol{H}$ and $\boldsymbol{G}$, respectively. Based on Theorem 1, by substituting (19) into the problem (10), the joint source and relay optimization problem (10) with complex-valued matrix variables is greatly simplified to the following optimal power allocation problem with non-negative scalar variables

$$\max_{\lambda_b,\boldsymbol{\lambda}_2,\boldsymbol{\lambda}_f,\alpha} \quad \frac{1-\alpha}{2}\min\left\{\sum_{i=1}^{R_h}\log_2(1+\sigma_r^{-2}\lambda_{h,i}\lambda_{2,i}),\ \sum_{j=1}^{R_g}\log_2(1+\sigma_d^{-2}\lambda_{g,j}\lambda_{f,j})\right\} \tag{20a}$$

$$\text{s.t. } \alpha\lambda_b+\frac{1-\alpha}{2}\sum_{i=1}^{R_h}\lambda_{2,i}\le\frac{1+\alpha}{2}P_s \tag{20b}$$

$$\sum_{j=1}^{R_g}\lambda_{f,j}\le\min\left\{\frac{2\alpha\eta}{1-\alpha}\lambda_{h,1}\lambda_b-N_rP_c,\ P_{m,r}\right\} \tag{20c}$$

$$0<\lambda_b\le P_{m,s},\quad \sum_{i=1}^{R_h}\lambda_{2,i}\le P_{m,s} \tag{20d}$$

$$0<\alpha<1,\quad \lambda_{2,i}\ge 0,\quad i=1\cdots,R_h \tag{20e}$$

$$\lambda_{f,j}\ge 0,\quad j=1,\cdots,R_g \tag{20f}$$

where $\boldsymbol{\lambda}_2=[\lambda_{2,1},\cdots,\lambda_{2,R_h}]^T$, $\boldsymbol{\lambda}_f=[\lambda_{f,1},\cdots,\lambda_{f,R_g}]^T$, $\lambda_{2,i}$ and $\lambda_{f,i}$ stand for the ith diagonal element of $\boldsymbol{\Lambda}_2$ and $\boldsymbol{\Lambda}_f$, respectively.

In Subsection III-A, we show that without the peak power constraints in (20c) and (20d), the power allocation problem (20) can be efficiently solved through a two-step approach following the unimodality of the objective function (20a). In particular, in the first step, we apply the golden section search to optimize the TS factor α. Then, in the second step, a two-loop bisection algorithm is developed to solve the power allocation problem with a fixed α. In Subsection III-B, we consider the peak transmission power constraints (20c) and (20d). By exploring the structure of the problem, we show that the power allocation problem with peak power constraints can be simplified into one or two subproblems which can be efficiently solved by the well-known water-filling algorithm.[4]

A. OPTIMAL SOLUTION WITHOUT PEAK POWER CONSTRAINTS

Without the peak power constraints in (20c) and (20d), the problem (20) is changed to the following problem

$$\max_{\lambda_b,\boldsymbol{\lambda}_2,\boldsymbol{\lambda}_f,\alpha} \quad \frac{1-\alpha}{2}\min\left\{\sum_{i=1}^{R_h}\log_2(1+\sigma_r^{-2}\lambda_{h,i}\lambda_{2,i}),\ \sum_{j=1}^{R_g}\log_2(1+\sigma_d^{-2}\lambda_{g,j}\lambda_{f,j})\right\} \tag{21a}$$

$$\text{s.t. } \alpha\lambda_b+\frac{1-\alpha}{2}\sum_{i=1}^{R_h}\lambda_{2,i}\le\frac{1+\alpha}{2}P_s \tag{21b}$$

$$\sum_{j=1}^{R_g}\lambda_{f,j}\le\frac{2\alpha\eta}{1-\alpha}\lambda_{h,1}\lambda_b-N_rP_c \tag{21c}$$

$$0<\alpha<1,\quad \lambda_{2,i}\ge 0,\quad i=1\cdots,R_h \tag{21d}$$

$$\lambda_{f,j}\ge 0,\quad j=1,\cdots,R_g. \tag{21e}$$

By introducing $P_\alpha=P_s\frac{1+\alpha}{1-\alpha}-\frac{N_rP_c}{\eta\lambda_{h,1}}$ and

$$a_i=\frac{\lambda_{h,i}}{\sigma_r^2},\ x_i=\lambda_{2,i},\quad i=1,\cdots,R_h \tag{22}$$

$$b_j=\frac{\eta\lambda_{g,j}\lambda_{h,1}}{\sigma_d^2},\ y_j=\frac{\lambda_{f,j}}{\eta\lambda_{h,1}},\quad j=1,\cdots,R_g \tag{23}$$

the problem (21) can be rewritten as

$$\max_{\alpha,\boldsymbol{x},\boldsymbol{y}} \quad \frac{1-\alpha}{2}\min\left\{\sum_{i=1}^{R_h}\log_2(1+a_ix_i),\ \sum_{j=1}^{R_g}\log_2(1+b_jy_j)\right\} \tag{24a}$$

$$\text{s.t. } \sum_{i=1}^{R_h}x_i+\sum_{j=1}^{R_g}y_j\le P_\alpha \tag{24b}$$

$$0<\alpha<1,\quad x_i\ge 0,\quad i=1,\cdots,R_h \tag{24c}$$

$$y_j\ge 0,\quad j=1,\cdots,R_g \tag{24d}$$

where $\boldsymbol{x}=[x_1,\cdots,x_{R_h}]^T$ and $\boldsymbol{y}=[y_1,\cdots,y_{R_g}]^T$. We assume that the static part of the circuit power consumption $N_rP_c<\eta\lambda_{h,1}P_s$ such that $P_\alpha>0$ for $0<\alpha<1$. The problem (24) is not a convex problem, because (24a) is not a concave function and (24b) is not a convex constraint. However, since $\min\{\sum_{i=1}^{R_h}\log_2(1+a_ix_i),\sum_{j=1}^{R_g}\log_2(1+b_jy_j)\}$ is a concave function of $\boldsymbol{x}$ and $\boldsymbol{y}$, the problem (24) is convex for a fixed α, which can be rewritten as

$$\max_{\boldsymbol{x},\boldsymbol{y},t} \quad t \tag{25a}$$

$$\text{tr}\ \sum_{i=1}^{R_h}\log_2(1+a_ix_i)\ge t \tag{25b}$$

$$\sum_{j=1}^{R_g}\log_2(1+b_jy_j)\ge t \tag{25c}$$

$$\sum_{i=1}^{R_h}x_i+\sum_{j=1}^{R_g}y_j\le P_\alpha \tag{25d}$$

$$x_i\ge 0, i=1,\cdots,R_h,\ y_j\ge 0, j=1,\cdots,R_g. \tag{25e}$$

The problem (25) is a convex problem. In fact, this problem maximizes the MI of a two-hop DF MIMO relay system with a sum power constraint across the source and relay nodes.

The Lagrangian function of the problem (25) can be written as

$$L=-t+\upsilon_1\left(t-\sum_{i=1}^{R_h}\log_2(1+a_ix_i)\right)+\upsilon_2\left(t-\sum_{j=1}^{R_g}\log_2(1+b_jy_j)\right)+\upsilon_3\left(\sum_{i=1}^{R_h}x_i+\sum_{j=1}^{R_g}y_j-P_\alpha\right).$$

[4]The proposed algorithms are carried out either at the source node or the destination node which have their own power supply and relatively higher computational capacity. The optimized variables such as $\boldsymbol{\lambda}_f$ are then forwarded to the relay node.

By considering the first order optimality condition, we have a water-filling solution as

$$\frac{\partial L}{\partial x_i} = 0 \longrightarrow x_i^* = \frac{1}{a_i}\left[\frac{\upsilon_1}{\upsilon_3}a_i - 1\right]^\dagger,\ i = 1, \cdots, R_h \quad (26)$$

$$\frac{\partial L}{\partial y_j} = 0 \longrightarrow y_j^* = \frac{1}{b_j}\left[\frac{\upsilon_2}{\upsilon_3}b_j - 1\right]^\dagger,\ j = 1, \cdots, R_g \quad (27)$$

where $[x]^\dagger = \max\{x, 0\}$. It can be seen from (26) and (27) that there must be $\upsilon_1 > 0$ and $\upsilon_2 > 0$, since otherwise, there are $x_i = 0$, $i = 1, \cdots, R_h$, and $y_j = 0$, $j = 1, \cdots, R_g$. From the complementary slackness condition this indicates that at the optimal solution, there is

$$\sum_{i=1}^{R_h} \log_2(1 + a_i x_i^*) = \sum_{j=1}^{R_g} \log_2(1 + b_j y_j^*) = t^*. \quad (28)$$

Therefore, the problem (25) can be solved by two loops of bisection as summarized in Algorithm 1, where the outer-loop is for finding the optimal t, and the inner-loop is to obtain the optimal $\boldsymbol{x}$ and $\boldsymbol{y}$, and ϵ is a positive constant close to 0.

Algorithm 1 Solving the Problem (25) through Two Loops of Bisection

Input: $P_\alpha, a_i, i = 1, \cdots, R_h, b_j, j = 1, \cdots, R_g$.
Output: $t^*, x_i^*, i = 1, \cdots, R_h, y_j^*, j = 1, \cdots, R_g$.
Initialization: The lower bound t_l and the upper bound t_u of t.
while $t_u - t_l > \epsilon$ **do**
  $t^* = (t_u + t_l)/2$.
  $x_i^* = \frac{1}{a_i}[\beta a_i - 1]^\dagger, i = 1, \cdots, R_h$.
  Find β by solving $\sum_{i=1}^{R_h} \log_2(1 + a_i x_i^*) = t^*$ using the bisection search method.
  $y_j^* = \frac{1}{b_j}[\gamma b_j - 1]^\dagger, j = 1, \cdots, R_g$.
  Find γ by solving $\sum_{j=1}^{R_g} \log_2(1 + b_j y_j^*) = t^*$ using the bisection search method.
  if $\sum_{i=1}^{R_h} x_i^* + \sum_{j=1}^{R_g} y_j^* > P_\alpha$ **then**
    Set $t_u = t^*$.
  else
    Set $t_l = t^*$.
  end if
end while

Since the problem (25) is convex and the left-hand sides of (25b)-(25d) are monotonically increasing functions of $\boldsymbol{x}$ and $\boldsymbol{y}$, Algorithm 1 is guaranteed to converge to the global optimum of the problem (25). The complexity of Algorithm 1 can be estimated as $\mathcal{O}(r_1 r_2 (R_h + R_g))$, where r_1 and r_2 are the number of iterations required by the outer bi-section loop and the inner bi-section loop till convergence, respectively.

Now we study the optimization of α and the solution of the problem (24). Let us denote the number of non-zero x_i^* in (26) as N_1 ($N_1 \le R_h$) and the number of non-zero y_j^* in (27) as N_2 ($N_2 \le R_g$).

Theorem 2: When $N_1 = N_2$ (equal number of active data streams in two hops), the objective function (24a) can be written as a closed-form function of α. This function is concave with respect to α.

Proof: See Appendix VI. ■

Based on Theorem 2, when $N_1 = N_2$, the optimal α in (24a) can be obtained via a simple one dimensional search. Then we can calculate the optimal t as (40) in Appendix VI. The optimal x_i and y_i can be obtained as (37) using the optimal β and γ in (38) of Appendix VI.

For the case of $N_1 \neq N_2$, as a closed-form expression of t^* in (28) is not available in general, (24a) cannot be written as a closed-form function of α. Nevertheless, through numerical simulations, we find that (24a) is always a unimodal function of α. Therefore, the problem (24) can be solved efficiently through a two-step approach. In particular, with a fixed α, $\boldsymbol{x}$ and $\boldsymbol{y}$ are optimized through solving the problem (25) following Algorithm 1. Then the golden section search [31] is adopted to find the optimal α. The steps of the two-step algorithm are listed in Algorithm 2, where $\varepsilon > 0$ is close to 0, $\delta = 1.618$ is the golden ratio [31], and $F(\alpha) = \frac{1-\alpha}{2}M(\alpha)$ is the objective function (24a). Here with a given α, $M(\alpha)$ is the maximal value of the problem (25). Finally, the optimal covariance matrices are obtained as Step 12 in Algorithm 2. The computational complexity of Algorithm 2 is given by $\mathcal{O}(r_1 r_2 r_3 (R_h + R_g))$, where r_3 is the number of golden section searches used to obtain the optimal α.

Algorithm 2 Procedure of Applying the Golden Section Search to Find the Optimal α and the Covariance Matrices.

Input: $P_s, \boldsymbol{H}, \boldsymbol{G}, a_i, i = 1, \cdots, R_h, b_j, j = 1, \cdots, R_g$.
Output: $\alpha^*, \boldsymbol{B}_1^*, \boldsymbol{B}_2^*, \boldsymbol{F}^*$.
Initialization: $\alpha_l = 0$ and $\alpha_u = 1$.
while $\alpha_u - \alpha_l \ge \varepsilon$ **do**
  Define $\nu_1 = (\delta - 1)\alpha_l + (2 - \delta)\alpha_u$ and $\nu_2 = (2 - \delta)\alpha_l + (\delta - 1)\alpha_u$.
  Solve the problem (25) for $\alpha = \nu_1$ using Algorithm 1; Calculate $F(\nu_1)$ for $\alpha = \nu_1$.
  Repeat Step 3 for $\alpha = \nu_2$.
  if $F(\nu_1) \le F(\nu_2)$ **then**
    Assign $\alpha_l = \nu_1$.
  else
    $\alpha_u = \nu_2$.
  end if
end while
$\alpha^* = (\alpha_u + \alpha_l)/2$.
Calculate $\lambda_{2,i}^* = x_i^*$, $i = 1, \cdots, R_h$, $\lambda_{f,j}^* = \eta y_j^* \lambda_{h,1}$, $j = 1, \cdots, R_g$, and $\lambda_b^* = \frac{1-\alpha^*}{2\alpha^*}\left(\sum_{j=1}^{R_g} y_j^* + \frac{N_r P_c}{\eta \lambda_{h,1}}\right)$. Then, calculate $\boldsymbol{B}_1^*, \boldsymbol{B}_2^*$, and $\boldsymbol{F}^*$ following (19).

B. OPTIMAL SOLUTION WITH PEAK TRANSMISSION POWER CONSTRAINTS

With peak transmission power constraints, for a fixed α, by using the variable substitutions in (22) and (23), the

problem (20) can be equivalently rewritten as

$$\max_{\boldsymbol{x},\boldsymbol{y},t} \quad t \tag{29a}$$

$$\text{s.t.} \quad \sum_{i=1}^{R_h} \log_2(1+a_i x_i) \geq t \tag{29b}$$

$$\sum_{j=1}^{R_g} \log_2(1+b_j y_j) \geq t \tag{29c}$$

$$\sum_{i=1}^{R_h} x_i + \sum_{j=1}^{R_g} y_j \leq P_\alpha \tag{29d}$$

$$\sum_{i=1}^{R_h} x_i \leq P_{m,s} \tag{29e}$$

$$\sum_{j=1}^{R_g} y_j \leq \min\left\{\frac{2\alpha P_{m,s}}{1-\alpha} - P_0, \frac{P_{m,r}}{\eta\lambda_{h,1}}\right\} \tag{29f}$$

$$x_i \geq 0, \quad i=1,\cdots,R_h, \quad y_j \geq 0, \quad j=1,\cdots,R_g \tag{29g}$$

where $P_0 = \frac{N_r P_c}{\eta\lambda_{h,1}}$, (29e) and (29f) are peak power constraints. It is easy to see that the problem (29) is convex. Interestingly, the problem (29) can be decomposed into the following two sub-problems. One sub-problem focuses on the optimization of the power allocation at the source as

$$\max_{\boldsymbol{x}} \quad \sum_{i=1}^{R_h} \log_2(1+a_i x_i) \tag{30a}$$

$$\text{s.t.} \quad \sum_{i=1}^{R_h} x_i \leq P_{m,s}, \quad x_i \geq 0, \quad i=1,\cdots,R_h. \tag{30b}$$

And the other sub-problem optimizes the power allocation at the relay as

$$\max_{\boldsymbol{y}} \quad \sum_{j=1}^{R_g} \log_2(1+b_j y_j) \tag{31a}$$

$$\text{s.t.} \quad \sum_{j=1}^{R_g} y_j \leq \min\left\{\frac{2\alpha P_{m,s}}{1-\alpha} - P_0, \frac{P_{m,r}}{\eta\lambda_{h,1}}\right\} \tag{31b}$$

$$y_j \geq 0, \quad j=1,\cdots,R_g. \tag{31c}$$

These two sub-problems are coupled by the constraint (29d). Note that both the problem (30) and the problem (31) are convex and can be solved by the well-known water-filling algorithm.

With these observations, the problem (29) can be solved by exploiting the solution of the problem (25). In particular, we first solve the problem (25) using Algorithm 1 and denote the output as t_0, $\boldsymbol{x}_0$, and $\boldsymbol{y}_0$. Then we check whether $\boldsymbol{x}_0$ and $\boldsymbol{y}_0$ satisfy (29e) and (29f), respectively. Firstly, if (29e) is satisfied by $\boldsymbol{x}_0$ and (29f) is satisfied by $\boldsymbol{y}_0$, obviously, in this case, t_0, $\boldsymbol{x}_0$, and $\boldsymbol{y}_0$ is the solution of the problem (29).

Secondly, (29e) is satisfied by $\boldsymbol{x}_0$, while $\boldsymbol{y}_0$ does not satisfy (29f). In this case, we solve the problem (31) and denote the solution as $\tilde{y}_j, j=1,\cdots,R_g$. The optimal value of (29a) is $\tilde{t} = \sum_{j=1}^{R_g} \log_2(1+b_j\tilde{y}_j)$. Thirdly, $\boldsymbol{y}_0$ satisfies (29f), while (29e) is violated by $\boldsymbol{x}_0$. In this scenario, we solve the problem (30) and denote its solution as $\tilde{x}_i$, $i=1,\cdots,R_h$. The optimal value of (29a) is $\tilde{t} = \sum_{i=1}^{R_h} \log_2(1+a_i\tilde{x}_i)$. Note that in both cases $\tilde{t} < t_0$.

Lastly, (29e) is violated by $\boldsymbol{x}_0$, and $\boldsymbol{y}_0$ does not satisfy (29f). For this case, we solve both the problem (30) and the problem (31) and take the smaller value of (30a) and (31a) as the optimal value of (29a). Following the discussions above, the procedure of solving the problem (29) is summarized in Algorithm 3.

Algorithm 3 Solving the Problem (29) Based on Algorithm 1

Input: $\alpha, P_{m,s}, P_{m,r}, a_i, i=1,\cdots,R_h, b_j, j=1,\cdots,R_g$.
Output: $t^*, x_i^*, i=1,\cdots,R_h, y_j^*, j=1,\cdots,R_g$.

1: Solve the problem (25) using Algorithm 1 and denote the output as t_0, $\boldsymbol{x}_0$, and $\boldsymbol{y}_0$.
2: Check (29e) and (29f) with $\boldsymbol{x}_0$ and $\boldsymbol{y}_0$, respectively.
3: **if** (29e) and (29f) are satisfied **then**
4: **return** $t^* = t_0, \boldsymbol{x}^* = \boldsymbol{x}_0$, and $\boldsymbol{y}^* = \boldsymbol{y}_0$.
5: **else if** (29e) is violated and (29f) is satisfied **then**
6: Find $\tilde{\boldsymbol{x}}$ by solving the problem (30).
7: **return** $t^* = \sum_{i=1}^{R_h} \log_2(1+a_i\tilde{x}_i), \boldsymbol{x}^* = \tilde{\boldsymbol{x}}$, and $\boldsymbol{y}^* = \boldsymbol{y}_0$.
8: **else if** (29f) is violated and (29e) is satisfied **then**
9: Find $\tilde{\boldsymbol{y}}$ by solving the problem (31).
10: **return** $t^* = \sum_{j=1}^{R_g} \log_2(1+b_j\tilde{y}_j), \boldsymbol{y}^* = \tilde{\boldsymbol{y}}$, and $\boldsymbol{x}^* = \boldsymbol{x}_0$.
11: **else**
12: Find $\tilde{\boldsymbol{x}}$ and $\tilde{\boldsymbol{y}}$ by solving the problem (30) and the problem (31), respectively.
13: **return** $t^* = \min\{\sum_{i=1}^{R_h} \log_2(1+a_i\tilde{x}_i), \sum_{j=1}^{R_g} \log_2(1+b_j\tilde{y}_j)\}, \boldsymbol{x}^* = \tilde{\boldsymbol{x}}$, and $\boldsymbol{y}^* = \tilde{\boldsymbol{y}}$.
14: **end if**

Similar to Algorithm 2, the problem (20) can be solved efficiently by a two-step approach. With a fixed α, $\boldsymbol{x}$ and $\boldsymbol{y}$ are optimized through solving the problem (29) following Algorithm 3. Then a golden section search is carried out to obtain the optimal α. It can be seen from Algorithm 3 that in the worst case, both the problem (30) and the problem (31) need to be solved. Thus, the worst-case complexity of Algorithm 3 is given by $\mathcal{O}((r_1 r_2 + r_4)(R_h + R_g))$, where r_4 is the number of bisection iterations used in solving the problem (30) and the problem (31). Since the complexity of computing the SVD of matrices $\boldsymbol{H}$ and $\boldsymbol{G}$ is $\mathcal{O}(N_s^2 N_r + N_r^3)$ and $\mathcal{O}(N_r^2 N_d + N_d^3)$, respectively, the total complexity order of solving the problem (10) is given by $\mathcal{O}(N_s^2 N_r + N_r^3 + N_r^2 N_d + N_d^3 + r_3(r_1 r_2 + r_4)(R_h + R_g))$.

IV. PROPOSED METHOD FOR THE PS BASED PROTOCOL

In this section, we study the joint optimization of the source and relay covariance matrices and the PS vector to maximize the source-destination MI in the PS based protocol.

Theorem 3: The covariance matrices $\boldsymbol{B}$ and $\boldsymbol{F}_p$ as the solution to the problem (18) has the following optimal structure

$$\boldsymbol{B}^* = \boldsymbol{V}_h \boldsymbol{\Lambda}_1 \boldsymbol{V}_h^H, \quad \boldsymbol{F}_p^* = \boldsymbol{V}_g \boldsymbol{\Lambda}_p \boldsymbol{V}_g^H \tag{32}$$

where $\boldsymbol{\Lambda}_1$ and $\boldsymbol{\Lambda}_p$ are $R_h \times R_h$ and $R_g \times R_g$ diagonal matrices, respectively.

Proof: See Appendix VI. ∎

From Theorem 3, we can see that the optimal $\boldsymbol{B}$ and $\boldsymbol{F}_p$ match the channel $\boldsymbol{H}$ and $\boldsymbol{G}$, respectively. By substituting (32) back into the problem (18), the transceiver optimization problem (18) with complex-valued matrix variables is reduced to the following power allocation problem with non-negative scalar variables

$$\max_{\boldsymbol{\lambda}_1, \boldsymbol{\lambda}_p, \boldsymbol{d}} \ \frac{1}{2} \min \left\{ \sum_{i=1}^{R_h} \log_2(1 + \sigma_r^{-2} \lambda_{h,i} \lambda_{1,i} d_i), \sum_{j=1}^{R_g} \log_2(1 + \sigma_d^{-2} \lambda_{g,j} \lambda_{p,j}) \right\} \tag{33a}$$

$$\text{s.t.} \ \sum_{i=1}^{R_h} \lambda_{1,i} \le P_s \tag{33b}$$

$$\sum_{j=1}^{R_g} \lambda_{p,j} \le \sum_{i=1}^{R_h} \eta(1 - d_i) \lambda_{h,i} \lambda_{1,i} - N_r P_c \tag{33c}$$

$$d_i \ge 0, \ \lambda_{1,i} \ge 0, \quad i = 1, \cdots, R_h \tag{33d}$$

$$\lambda_{p,j} \ge 0, \ j = 1, \cdots, R_g \tag{33e}$$

where $\boldsymbol{\lambda}_1 = [\lambda_{1,1}, \cdots, \lambda_{1,R_h}]^T$, $\boldsymbol{\lambda}_p = [\lambda_{p,1}, \cdots, \lambda_{p,R_g}]^T$, and $\boldsymbol{d} = [d_1, \cdots, d_{R_h}]^T$. Since due to path loss, $\lambda_{h,i} < 1$, we have $\sum_{i=1}^{R_h} \eta(1 - d_i) \lambda_{h,i} \lambda_{1,i} < \sum_{i=1}^{R_h} \lambda_{1,i} \le P_s$. Thus, there is no need to impose peak power constraint at the relay node. By introducing $q_i = d_i \lambda_{1,i}$, $i = 1, \cdots, R_h$, the problem (33) can be converted to

$$\max_{\boldsymbol{\lambda}_1, \boldsymbol{\lambda}_p, \boldsymbol{q}, t} \ \frac{1}{2} t \tag{34a}$$

$$\text{s.t.} \ \sum_{i=1}^{R_h} \log_2(1 + \sigma_r^{-2} \lambda_{h,i} q_i) \ge t \tag{34b}$$

$$\sum_{j=1}^{R_g} \log_2(1 + \sigma_d^{-2} \lambda_{g,j} \lambda_{p,j}) \ge t \tag{34c}$$

$$\sum_{i=1}^{R_h} \lambda_{1,i} \le P_s \tag{34d}$$

$$\sum_{j=1}^{R_g} \lambda_{p,j} \le \sum_{i=1}^{R_h} \eta \lambda_{h,i} (\lambda_{1,i} - q_i) - N_r P_c \tag{34e}$$

$$\lambda_{1,i} \ge q_i \ge 0, \quad i = 1, \cdots, R_h \tag{34f}$$

$$\lambda_{p,j} \ge 0, \quad j = 1, \cdots, R_g \tag{34g}$$

where $\boldsymbol{q} = [q_1, \cdots, q_{R_h}]^T$. Here, we develop an interior point method based algorithm following the steps in Algorithm 11.2 of [39] to solve the problem (34).

The procedure of applying the primal-dual interior point method to solve the problem (34) is summarized in Algorithm 4, where $\boldsymbol{e} = [\boldsymbol{\lambda}_1^T, \boldsymbol{\lambda}_p^T, \boldsymbol{q}^T, t]^T$ is the primal variable vector, $\boldsymbol{\mu} = [\mu_1, \cdots, \mu_{2R_h+R_g+4}]^T$ denotes the dual variable vector, $\|\cdot\|_2$ stands for the vector Euclidean norm, $\boldsymbol{g}(\boldsymbol{e})$, $\boldsymbol{r}_d(\boldsymbol{e}, \boldsymbol{\mu})$, and $\boldsymbol{r}_c(\boldsymbol{e}, \boldsymbol{\mu})$ are defined in (46), (48), and (49), respectively. Here, the Newton search direction of the primal and dual variables is derived in Appendix VI.

Algorithm 4 Solving the Problem (34) by the Primal-dual Interior Point Method

Input: $\eta, \sigma_r, \sigma_d, P_s, \lambda_{h,i}, i = 1, \cdots, R_h, \lambda_{g,j}, j = 1, \cdots, R_g$.
Output: $\lambda_{1,i}, q_i, i = 1, \cdots, R_h, \lambda_{p,j}, j = 1, \cdots, R_g$.

Initialization: The primal feasible tolerance ϵ_p, the dual feasible tolerance ϵ_d, $\rho > 1$, $\tau \in [0.3, 0.8]$, $\phi \in [0.01, 0.1]$, and the initial primal and dual variables $\boldsymbol{e}$ and $\boldsymbol{\mu}$.

Calculate $\boldsymbol{r}_d(\boldsymbol{e}, \boldsymbol{\mu})$ and $\kappa = -\boldsymbol{g}(\boldsymbol{e})^T \boldsymbol{\mu}$.
while $\|\boldsymbol{r}_d(\boldsymbol{e}, \boldsymbol{\mu})\|_2 > \epsilon_d$ and $\kappa > \epsilon_p$ **do**
  Calculate $\omega = (2R_h + R_g + 4)\rho/\kappa$ in (49) of Appendix VI.
  Obtain the Newton search direction $[\Delta \boldsymbol{e}^T, \Delta \boldsymbol{\mu}^T]^T$ by solving (47) in Appendix VI.
  Compute $\xi = 0.99 \min\{1, \min\{-\mu_i / \Delta\mu_i | \Delta\mu_i < 0\}\}$.
  Let $\boldsymbol{e}^* = \boldsymbol{e}$.
  while $\boldsymbol{g}(\boldsymbol{e}^*) \ge \boldsymbol{0}_{(2R_h+R_g+4)\times 1}$ **do**
    $\xi := \tau \xi$.
    $\boldsymbol{e}^* = \boldsymbol{e} + \xi \Delta \boldsymbol{e}$.
  end while
  Let $\boldsymbol{\mu}^* = \boldsymbol{\mu}$.
  while $\|[\boldsymbol{r}_d(\boldsymbol{e}^*, \boldsymbol{\mu}^*)^T, \boldsymbol{r}_c(\boldsymbol{e}^*, \boldsymbol{\mu}^*)^T]^T\|_2 > (1 - \phi\xi) \times \|[\boldsymbol{r}_d(\boldsymbol{e}, \boldsymbol{\mu})^T, \boldsymbol{r}_c(\boldsymbol{e}, \boldsymbol{\mu})^T]^T\|_2$ **do**
    $\xi := \tau \xi$.
    $\boldsymbol{\mu}^* = \boldsymbol{\mu} + \xi \Delta \boldsymbol{\mu}$.
  end while
  Let $[\boldsymbol{e}_o^T, \boldsymbol{\mu}_o^T]^T = [\boldsymbol{e}^T, \boldsymbol{\mu}^T]^T + \xi [\Delta \boldsymbol{e}^T, \Delta \boldsymbol{\mu}^T]^T$.
  Set $\boldsymbol{e} = \boldsymbol{e}_o$, $\boldsymbol{\mu} = \boldsymbol{\mu}_o$, and $\kappa = -\boldsymbol{g}(\boldsymbol{e})^T \boldsymbol{\mu}$.
end while

As the problem (34) is convex, the primal-dual interior point method in Algorithm 4 is guaranteed to converge to the global optimum of the problem (34). Since the main computation load in each primal-dual search is the calculation of the inverse of a $(4R_h + 2R_g + 5) \times (4R_h + 2R_g + 5)$ matrix to solve the equation (47), the computational complexity of Algorithm 4 is $\mathcal{O}(r_5(4R_h + 2R_g + 5)^3)$, where r_5 is the number of iterations till convergence. Thus, the total computational complexity order of solving the problem (18) is $\mathcal{O}(N_s^2 N_r + N_r^3 + N_r^2 N_d + N_d^3 + r_5(4R_h + 2R_g + 5)^3)$. It can be seen that the complexity of the PS based protocol is higher than that of the TS based protocol. However, it will be shown in the next section that the PS based protocol yields a higher system MI than the TS based protocol.

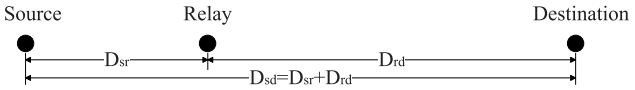

FIGURE 4. Source, relay, and destination placement.

V. SIMULATIONS

In this section, we investigate the performance of TS based and PS based protocols through numerical simulations. We simulate a scenario where the source, relay, and destination nodes are located in a line as shown in Fig. 4. The source-destination distance is $D_{sd} = 20$ meters (m), and the source-relay and relay-destination distances are $D_{sr} = 10k$ m and $D_{rd} = 10(2-k)$ m, respectively, where the value of $0 < k < 2$ is normalized over a distance of 10 meters. Note that this is among the typical distance of RF-based wireless power transfer reported in [40], and this simulation scenario is chosen to make it easy to study the system performance with respect to the location of the relay node. In the simulations, we choose $0.1 < k < 1.9$ such that $D_{sr} > 1$ and $D_{rd} > 1$.

Similar to [27] and [28], we model the channel matrices as $\boldsymbol{H} = D_{sr}^{-\zeta/2}\bar{\boldsymbol{H}}$ and $\boldsymbol{G} = D_{rd}^{-\zeta/2}\bar{\boldsymbol{G}}$, where $D_{sr}^{-\zeta}$ and $D_{rd}^{-\zeta}$ stand for the large-scale path loss with ζ being the path loss exponent, and $\bar{\boldsymbol{H}}$ and $\bar{\boldsymbol{G}}$ represent the small-scale Rayleigh channel fading. We simulate the suburban communication environment with $\zeta = 3$. Entries of $\bar{\boldsymbol{H}}$ and $\bar{\boldsymbol{G}}$ have independent and identical complex Gaussian distribution with zero-mean and variances of $1/N_s$ and $1/N_r$, respectively. The relay and the destination noise variances are set as $\sigma_r^2 = \sigma_d^2 = -50$ dBm. We set the per-antenna static power consumption at the relay node as $P_c = 1\mu$W [41].

In the simulations, we set $\eta = 0.7$ [1] and $N_s = N_r = N_d = N$, unless explicitly mentioned. We compare the performance of the TS based protocol and the PS based protocol with the wireless powered AF MIMO relay system [30]. For the TS based protocol with peak transmission power constraints, we set $P_{m,s} = P_{m,r} = \theta P_s$ in the simulations ($\theta \geq 1$). All numerical results are averaged through 1000 independent channel realizations.

A. EXAMPLE 1: MI VERSUS THE NOMINAL SOURCE NODE POWER

In the first example, we set $k = 1$ and $\theta = 1$. The system MI of the four systems tested versus the nominal source node power P_s for $N = 3$ and $N = 5$ is illustrated tin Fig. 5 and Fig. 6, respectively. From Figs. 5 and 6, we observe that the PS based protocol yields a slightly higher MI than the TS based protocol without peak power constraints at low P_s, and both protocols have a higher MI than the AF MIMO relay system without peak power constraints in [30]. The reason is that for the AF scheme, the noise at the relay node is amplified and forwarded to the destination node, while a DF relay stops such noise propagation. Note that the TS based protocol has a similar complexity order as that of the AF MIMO relay system. It can also be observed from Figs. 5 and 6 that the MI by the TS based protocol with peak power constraints is lower

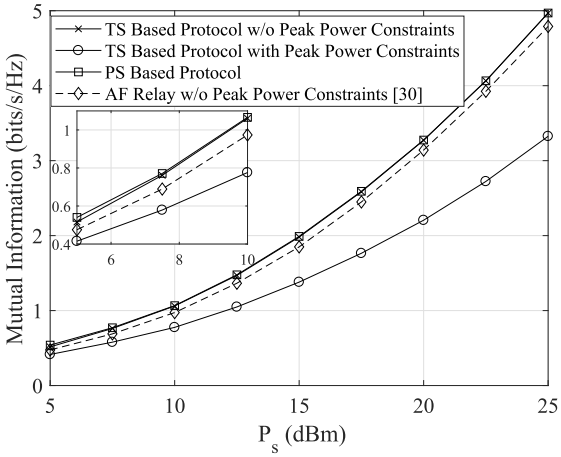

FIGURE 5. Example 1: MI versus P_s, $N = 3$, $k = 1$, and $\theta = 1$.

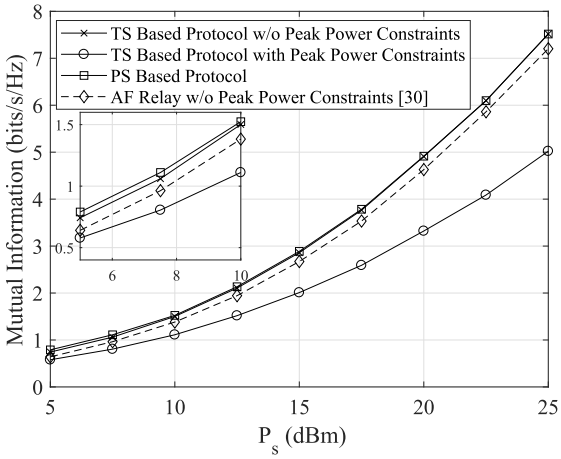

FIGURE 6. Example 1: MI versus P_s, $N = 5$, $k = 1$, and $\theta = 1$.

than that without peak power constraints. This is because the feasible region of the former system is smaller than that of the latter one. By comparing Fig. 5 with Fig. 6, we can observe that for all three protocols, the relay system with $N = 5$ has a higher MI than that of the system with $N = 3$. This is due to the benefits of the MIMO technology.

B. EXAMPLE 2: TS BASED PROTOCOL WITH DIFFERENT PEAK TRANSMISSION POWER CONSTRAINTS

We choose $N = 3$ and $k = 1$ in the second example. We plot the MI of the TS based protocol versus the nominal source node power P_s with various peak power constraints at $\theta = 1$, $\theta = 2$, and $\theta = 10$ in Fig. 7. As shown in Fig. 7, the achievable system MI of the TS based protocol with peak power constraints increases as the power limits $P_{m,s}$ and $P_{m,r}$ increase. When the power limits are sufficiently large (e.g. $\theta = 10$), the achievable MI is almost identical to that of the TS based protocol without peak power constraints. This is because the peak power constraints are easily satisfied when the power limits are high. We also see from Fig. 7 that

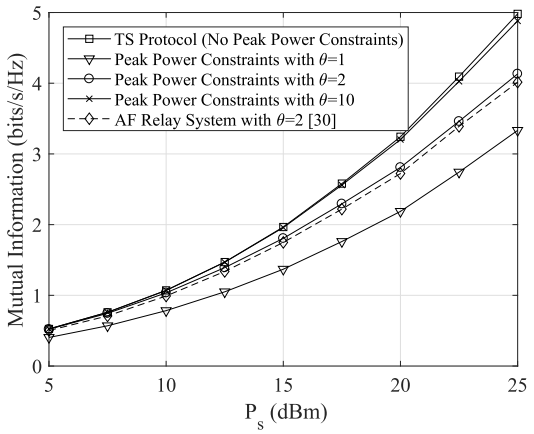

FIGURE 7. Example 2: MI versus P_s, $N = 3$ and $k = 1$.

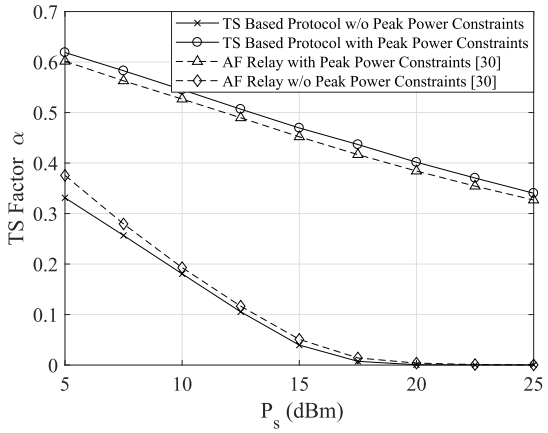

FIGURE 8. Example 3: TS factor versus P_s, $N = 5$, $k = 1$, and $\theta = 1$.

for $\theta = 2$, the proposed TS based protocol attains a higher MI than the AF MIMO relay system.

C. EXAMPLE 3: OPTIMAL α OF THE TS BASED PROTOCOL WITH AND WITHOUT PEAK POWER CONSTRAINTS

In this example, we set $N = 5$, $k = 1$, $\theta = 1$, and plot the optimal α of the TS based protocol and the AF MIMO relay system in [30] (both with and without peak power constraints) versus P_s in Fig. 8. We can observe from Fig. 8 that for the TS based protocol and the AF MIMO relay system without peak power constraints, the optimal value of α decreases monotonically as the source node power P_s increases. Interestingly, the optimal α has a very small value when P_s is high. This is due to the fact that as P_s increases, without the source node peak power limit, a smaller α is sufficient to harvest enough energy at the relay node required to forward the information signals due to the high power received at the first time interval. Then, more time can be spent on transmitting the information signals. In contrast, the optimal α for the TS based protocol and the AF MIMO relay system with peak power constraints does not decrease to a very small value when P_s increases. This is due to the fact

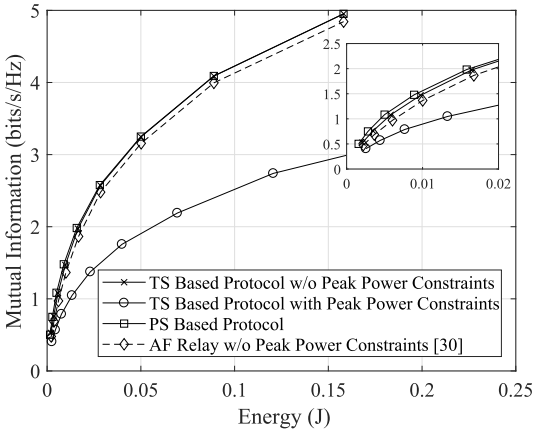

FIGURE 9. Example 4: MI versus energy consumption, $N = 3$, $k = 1$, and $\theta = 1$.

that the power constraint limits the power transferred from the source node to the relay node during the first interval, and thus a larger α is needed for the relay node to harvest sufficient energy. Interestingly, we observe from Fig. 8 that the proposed TS protocol has a smaller α than the AF MIMO relay system without peak power constraints. But with peak power constraints, the latter one has a smaller α.

D. EXAMPLE 4: MI AND ENERGY CONSUMPTION TRADE-OFF COMPARISONS

We set $N = 3$, $k = 1$, and $\theta = 1$ in this simulation example. The achievable MI versus the energy consumption at the source node is plotted in Fig. 9. We can observe from Fig. 9 that the PS based protocol and the TS protocol without peak power constraints obtain a similar MI and energy trade-off, with the former one achieving a little higher MI at low energy levels. Both of them have a higher MI than the AF MIMO relay system. Thus, the proposed systems have a higher energy efficiency. As expected, for a given energy consumption, the TS based protocol without peak power constraints achieves a larger MI than the system with peak power constraints.

For this example, we also plot the energy consumption versus P_s in Fig. 10. We can see from Fig. 10 that the energy power trade-off for the TS protocol without peak power constraints and the PS based protocol is very similar in the mid-and-high range of P_s, while the latter one consumes less energy at low P_s. This is because for the TS based protocol, the time duration for the energy and information transfer from the source node to the relay node is $\frac{1+\alpha}{2}$. From Fig. 8, we know that the optimal α is close to 0 in the mid-and-high range of P_s for the TS based protocol without peak power constraints. Thus, the time duration is close to $\frac{1}{2}$, which is the same time duration for the PS based protocol. Therefore, the energy consumption for these two protocols are almost the same in Fig. 10. In contrast, we observe that the optimal α is large in Fig. 8 for the TS based protocol with peak power constraints. Thus, its energy consumption is larger than the other two protocols.

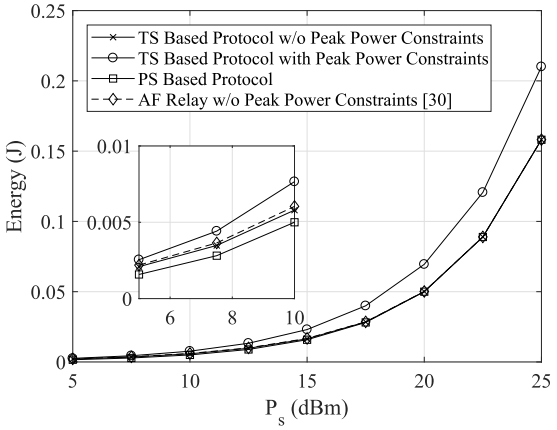

FIGURE 10. Example 4: Energy consumption versus P_S, $N = 3$, $k = 1$, and $\theta = 1$.

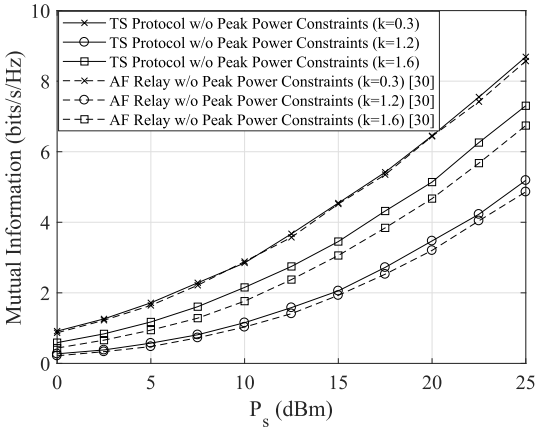

FIGURE 12. Example 5: MI versus P_S for the TS based protocol without peak power constraints at different k, $N = 3$.

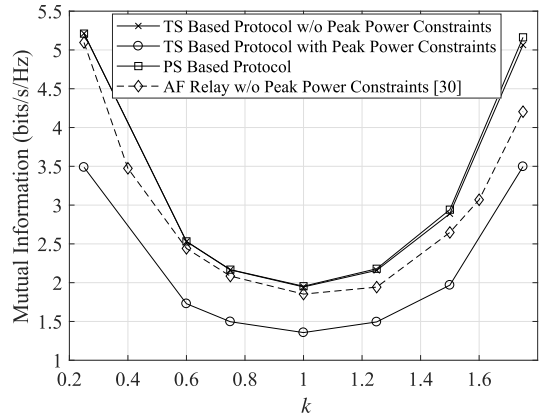

FIGURE 11. Example 5: MI versus k, $N = 3$, $\theta = 1$, and $P_S = 15$ dBm.

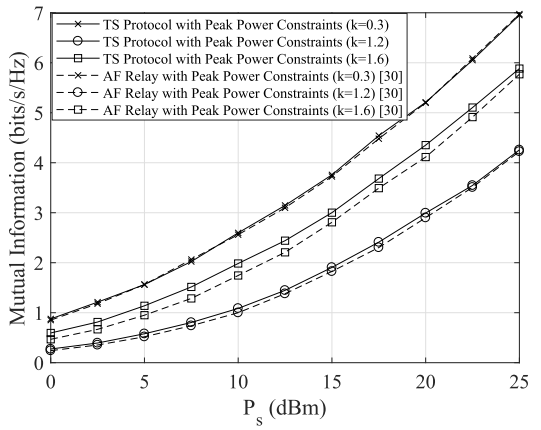

FIGURE 13. Example 5: MI versus P_S for the TS protocol with peak transmission power constraints at different k, $N = 3$, and $\theta = 1$.

E. EXAMPLE 5: ACHIEVABLE MI AT VARIOUS LOCATIONS OF THE RELAY NODE

In this example, we investigate the MI achievable at different k. We set $N = 3$, $\theta = 1$, $P_s = 15$ dBm, and plot the MI versus k for the four systems tested in Fig. 11. It can be observed from Fig. 11 that for the four systems, the system MI first decreases and then increases as k increases. This is because when the relay node is located closer to the source node, more energy can be harvested leading to a higher MI. When the relay node is located very close to the destination node, although the amount of harvested energy is smaller, a better second-hop channel due to the shorter relay-destination distance improves the system MI. It can also be seen from Fig. 11 that the PS based protocol and the TS protocol without peak power constraints have similar MIs for $k \leq 1$, and the former one yields a slightly higher MI when $k > 1$. Both protocols yield a higher MI than the AF MIMO relay system for the whole range of k.

To test the performance of the three protocols at various locations of the relay node, we plot the system MI versus P_s at various k for the TS based protocol without peak power constraints, the TS based protocol with peak power constraints, and the PS based protocol in Fig. 12, Fig. 13, and Fig. 14, respectively. It can be observed from Fig. 12-Fig. 14 that similar to Fig. 11, the system MI first decreases and then increases again when k increases. We also observe from Figs. 12 and 13 that the TS based protocol attains a higher MI than the AF MIMO relay system.

F. EXAMPLE 6: IMPACT OF ANTENNA DISTRIBUTIONS AT THREE NODES ON THE SYSTEM MI

In the last example, we consider a MIMO relay system with a fixed total number of antennas $N_s + N_r + N_d = M$ and study how the distribution of the number of antennas at each node affects the system MI. We set $M = 9$ and $k = 1$. Fig. 15 shows the system MI of the TS protocol without peak power constraints versus P_s at various combinations of (N_s, N_r, N_d). It can be observed from Fig. 15 that the highest MI is achieved by $N_s = 2, N_r = 3, N_d = 4$, while the lowest MI is obtained from $N_s = 4, N_r = 3, N_d = 2$. This indicates that for a given M, the system MI benefits from allocating more antennas to the destination node. The reason can be explained below. As the relay node is powered by harvesting

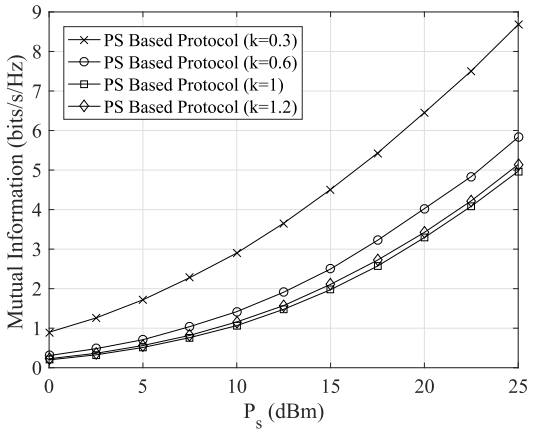

FIGURE 14. Example 5: MI versus P_S for the PS based protocol at different k, $N = 3$.

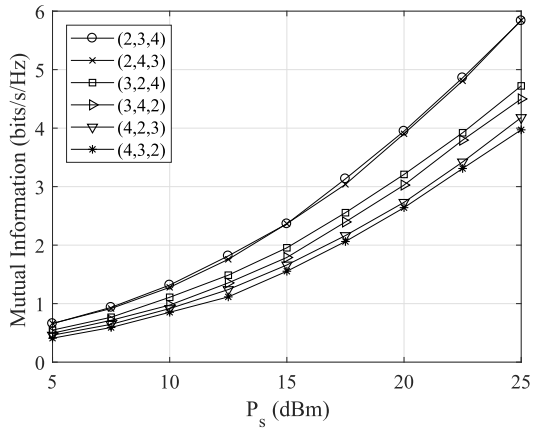

FIGURE 15. Example 6: MI versus P_S for the TS protocol without peak power constraints at various (N_s, N_r, N_d), $M = 9$ and $k = 1$.

the RF energy from the source node, the transmission power at the relay node is smaller than that of the source node. Thus, the system MI is limited by the MI of the second-hop channel, and it is sensible to have a larger number of destination antennas to improve the MI of the second-hop channel.

VI. CONCLUSIONS

We have studied the joint source and relay optimization for wireless powered two-hop DF MIMO relay systems. Both the TS based protocol and the PS based protocol have been investigated. For each protocol, the optimal structure of the source and relay covariance matrices has been derived, which reduces the original problems to simpler power allocation problems. A two-step optimization method has been proposed for the TS based protocol. We have proven that for a given TS factor, the power allocation problem is convex and a two-loop bisection algorithm has been proposed to solve the problem. We have also considered practical peak power constraints in the TS protocol. A decomposition based algorithm has been developed to simplify the power allocation problem with peak transmission power constraints into one or two simpler problems which can be solved by the water-filling algorithm. For the PS based protocol, an efficient primal-dual interior point method based algorithm has been proposed to solve the optimal power allocation problem. Numerical simulations demonstrate that the proposed DF relay system has a higher MI than the AF relay system. Interestingly, the PS based protocol achieves a higher system MI at a higher computational complexity. The optimal TS factor decreases with the source power. With peak transmission power constraints, the optimal TS factor does not change too much. We have found that the achievable system MI is lower as the relay node is allocated halfway between the source and destination nodes.

APPENDIX A
PROOF OF THEOREM 1

We first prove the structure of the optimal $\boldsymbol{B}_1$. We can observe from the problem (10) that as $\boldsymbol{B}_1$ is not in (10a), it changes the value of (10a) by varying the feasible region of the problem given by the constraints (10b)-(10d). Thus, to maximize the feasible region of (10b)-(10d), for *any* $\mathrm{tr}(\boldsymbol{B}_1)$, we should maximize $\mathrm{tr}(\boldsymbol{H}\boldsymbol{B}_1\boldsymbol{H}^H)$, which can be written as the following optimization problem

$$\max_{\boldsymbol{B}_1\succeq 0} \ \mathrm{tr}(\boldsymbol{H}\boldsymbol{B}_1\boldsymbol{H}^H) \tag{35a}$$

$$\text{s.t. } \mathrm{tr}(\boldsymbol{B}_1) = \lambda_b \tag{35b}$$

where $\lambda_b > 0$. Based on Proposition 2.1 of [5], the optimal $\boldsymbol{B}_1$ in the problem (35) must satisfy $\boldsymbol{B}_1^* = \lambda_b \boldsymbol{v}_{h,1}\boldsymbol{v}_{h,1}^H$. By substituting $\boldsymbol{B}_1^*$ into the problem (10), we obtain the following problem

$$\max_{\alpha,\lambda_b,\boldsymbol{B}_2\succeq 0,\boldsymbol{F}\succeq 0} \ \mathrm{MI}(\alpha,\boldsymbol{B}_2,\boldsymbol{F}) \tag{36a}$$

$$\text{s.t. } \mathrm{tr}(\boldsymbol{B}_2) \le \min\left\{\frac{2}{1-\alpha}\left(\frac{1+\alpha}{2}P_s - \alpha\lambda_b\right), P_{m,s}\right\} \tag{36b}$$

$$\mathrm{tr}(\boldsymbol{F}) \le \min\left\{\frac{2\alpha\eta\lambda_b}{1-\alpha}\lambda_{h,1} - N_r P_c, P_{m,r}\right\} \tag{36c}$$

$$\lambda_b \le P_{m,s}, \quad 0 < \alpha < 1. \tag{36d}$$

Obviously, the optimal $\boldsymbol{B}_2$ for the problem (36) should maximize $\log_2|\boldsymbol{I}_{N_r} + \sigma_r^{-2}\boldsymbol{H}\boldsymbol{B}_2\boldsymbol{H}^H|$ subjecting to (36b). Thus, for *any* α and λ_b, we have $\boldsymbol{B}_2^* = \boldsymbol{V}_h\boldsymbol{\Lambda}_2\boldsymbol{V}_h^H$. Similarly, the optimal $\boldsymbol{F}$ should maximize $\log_2|\boldsymbol{I}_{N_d} + \sigma_d^{-2}\boldsymbol{G}\boldsymbol{F}\boldsymbol{G}^H|$ subjecting to (36c), leading to $\boldsymbol{F}^* = \boldsymbol{V}_g\boldsymbol{\Lambda}_f\boldsymbol{V}_g^H$ for *any* α and λ_b.

APPENDIX B
PROOF OF THEOREM 2

Let us denote $N_1 = N_2 = N_0$. From (26) and (27), we have

$$x_i^* = \frac{\beta a_i - 1}{a_i}, \quad y_i^* = \frac{\gamma b_i - 1}{b_i}, \quad i = 1, \cdots, N_0. \tag{37}$$

By substituting (37) back into (28), we obtain

$$\beta = 2^{\frac{t^* - \sum_{i=1}^{N_0}\log_2 a_i}{N_0}}, \quad \gamma = 2^{\frac{t^* - \sum_{i=1}^{N_0}\log_2 b_i}{N_0}}. \tag{38}$$

From (37) and the power constraint (24b), we have

$$\sum_{i=1}^{N_0}\left(\beta-\frac{1}{a_i}+\gamma-\frac{1}{b_i}\right)=P_\alpha. \tag{39}$$

By substituting (38) into (39), we obtain

$$t^*=N_0\log_2\frac{c_1c_2w}{c_1+c_2} \tag{40}$$

where

$$c_1=\prod_{i=1}^{N_0}a_i^{\frac{1}{N_0}},\quad c_2=\prod_{i=1}^{N_0}b_i^{\frac{1}{N_0}},\quad w=\frac{1}{N_0}\left[P_\alpha+\sum_{i=1}^{N_0}\left(\frac{1}{a_i}+\frac{1}{b_i}\right)\right].$$

From (40), the achievable system MI (24a) is to maximize $\frac{1-\alpha}{2}t^*$, which is given by

$$\max_{0<\alpha<1}\quad\frac{(1-\alpha)N_0}{2}\log_2\left(\frac{1+\alpha}{1-\alpha}k_1+k_2\right) \tag{41}$$

where

$$k_1=\frac{c_1c_2P_s}{(c_1+c_2)N_0},\quad k_2=\frac{c_1c_2}{N_0(c_1+c_2)}\sum_{i=1}^{N_0}\left(\frac{1}{a_i}+\frac{1}{b_i}\right).$$

Let $f(\alpha)=\frac{(1-\alpha)N_0}{2}\log_2(\frac{1+\alpha}{1-\alpha}k_1+k_2)$. It can be shown that

$$\frac{d^2f(\alpha)}{d\alpha^2}=\frac{2k_1^2}{(\ln 2)N_0((k_1-k_2)\alpha+k_1+k_2)^2(\alpha-1)}\le 0.$$

Therefore, $f(\alpha)$, and thus (24a), is a concave function of α.

APPENDIX C
PROOF OF THEOREM 3

First we prove that the optimal structure of $\boldsymbol{B}$ in (32) maximizes the right-hand side of (18c), which is cast as the problem below

$$\max_{\boldsymbol{B}\succeq 0}\ \mathrm{tr}((\boldsymbol{I}_{R_h}-\boldsymbol{D})\boldsymbol{\Lambda}_h^{\frac{1}{2}}\boldsymbol{V}_h^H\boldsymbol{B}\boldsymbol{V}_h\boldsymbol{\Lambda}_h^{\frac{1}{2}}) \tag{42a}$$

$$\text{s.t. } \mathrm{tr}(\boldsymbol{B})\le P_s. \tag{42b}$$

By introducing $\tilde{\boldsymbol{D}}=(\boldsymbol{I}_{R_h}-\boldsymbol{D})\boldsymbol{\Lambda}_h$, the problem (42) can be rewritten as

$$\max_{\boldsymbol{B}\succeq 0}\ \mathrm{tr}(\boldsymbol{V}_h\tilde{\boldsymbol{D}}\boldsymbol{V}_h^H\boldsymbol{B}) \tag{43a}$$

$$\text{s.t. } \mathrm{tr}(\boldsymbol{B})\le P_s. \tag{43b}$$

Since $\tilde{\boldsymbol{D}}$ is diagonal, from Proposition 2.1 of [5], the solution to the problem (43) satisfies $\boldsymbol{B}^*=P_s\boldsymbol{v}_{h,1}\boldsymbol{v}_{h,1}^H$. Obviously, this is a special case of $\boldsymbol{B}^*=\boldsymbol{V}_h\boldsymbol{\Lambda}_1\boldsymbol{V}_h^H$ in (32).

Secondly, for *any* $\boldsymbol{D}$ and $\boldsymbol{B}$, let us denote $\eta\mathrm{tr}((\boldsymbol{I}_{R_h}-\boldsymbol{D})\tilde{\boldsymbol{B}})-N_rP_c=P_r$. Then the problem (18) can be rewritten as

$$\max_{\boldsymbol{D},\boldsymbol{B}\succeq 0,\boldsymbol{F}_p\succeq 0}\ \mathrm{MI}(\boldsymbol{D},\boldsymbol{B},\boldsymbol{F}_p) \tag{44a}$$

$$\text{s.t. } \mathrm{tr}(\boldsymbol{B})\le P_s \tag{44b}$$

$$\mathrm{tr}(\boldsymbol{F}_p)\le P_r. \tag{44c}$$

We can easily see from the problem (44) that the optimal $\boldsymbol{B}$ should maximize $\log_2|\boldsymbol{I}_{R_h}+\sigma_r^{-2}\boldsymbol{D}^{\frac{1}{2}}\tilde{\boldsymbol{B}}\boldsymbol{D}^{\frac{1}{2}}|$ subjecting to (44b). Thus, for *any* $\boldsymbol{D}$, we have $\boldsymbol{B}^*=\boldsymbol{V}_h\boldsymbol{\Lambda}_1\boldsymbol{V}_h^H$. The optimal $\boldsymbol{F}_p$ should maximize $\log_2|\boldsymbol{I}_{R_g}+\sigma_d^{-2}\boldsymbol{G}\boldsymbol{F}_p\boldsymbol{G}^H|$ subjecting to (44c), which is given by $\boldsymbol{F}_p^*=\boldsymbol{V}_g\boldsymbol{\Lambda}_p\boldsymbol{V}_g^H$ for *any* $\boldsymbol{D}$ and $\boldsymbol{B}$.

APPENDIX D
THE NEWTON SEARCH DIRECTION OF THE PROBLEM (34)

By omitting the constant factor $1/2$ in (34a), the problem (34) can be rewritten into a more compact form as

$$\max_{\boldsymbol{e}}\ t \tag{45a}$$

$$\text{s.t. } \boldsymbol{g}(\boldsymbol{e})\le\boldsymbol{0}_{(2R_h+R_g+4)\times 1} \tag{45b}$$

where

$$\boldsymbol{g}(\boldsymbol{e})=\begin{bmatrix} t-\sum_{i=1}^{R_h}\log_2(1+\sigma_r^{-2}\lambda_{h,i}q_i)\\ t-\sum_{j=1}^{R_g}\log_2(1+\sigma_d^{-2}\lambda_{g,j}\lambda_{p,j})\\ \sum_{i=1}^{R_h}\lambda_{1,i}-P_s\\ \sum_{j=1}^{R_g}\lambda_{p,j}-\sum_{i=1}^{R_h}\eta\lambda_{h,i}(\lambda_{1,i}-q_i)+N_rP_c\\ \boldsymbol{q}-\boldsymbol{\lambda}_1\\ -\boldsymbol{\lambda}_p\\ -\boldsymbol{q}\end{bmatrix}. \tag{46}$$

The Newton search direction $[\Delta\boldsymbol{e}^T,\Delta\boldsymbol{\mu}^T]^T$ is obtained based on the linearization of the modified Karush-Kuhn-Tucker (KKT) conditions, which can be obtained by solving the following equation

$$\begin{bmatrix}\nabla^2 g_0(\boldsymbol{e})+\sum_{i=1}^{2R_h+R_g+4}\mu_i\nabla^2 g_i(\boldsymbol{e}) & D\boldsymbol{g}(\boldsymbol{e})^T\\ -\mathrm{diag}(\boldsymbol{\mu})D\boldsymbol{g}(\boldsymbol{e}) & -\mathrm{diag}(\boldsymbol{g}(\boldsymbol{e}))\end{bmatrix}\begin{bmatrix}\Delta\boldsymbol{e}\\ \Delta\boldsymbol{\mu}\end{bmatrix}=-\begin{bmatrix}\boldsymbol{r}_d(\boldsymbol{e},\boldsymbol{\mu})\\ \boldsymbol{r}_c(\boldsymbol{e},\boldsymbol{\mu})\end{bmatrix} \tag{47}$$

where $\nabla^2 g_0(\boldsymbol{e})$ is the second-order derivative matrix of the object function (45a) given by

$$\nabla^2 g_0(\boldsymbol{e})=\boldsymbol{0}_{(2R_h+R_g+1)\times(2R_h+R_g+1)}.$$

In (47), $D\boldsymbol{g}(\boldsymbol{e})$ is the first-order derivative matrix of $\boldsymbol{g}(\boldsymbol{e})$ as

$$D\boldsymbol{g}(\boldsymbol{e})=\begin{bmatrix}\boldsymbol{0}_{1\times R_h} & \boldsymbol{0}_{1\times R_g} & \boldsymbol{m} & 1\\ \boldsymbol{0}_{1\times R_h} & \boldsymbol{n} & \boldsymbol{0}_{1\times R_h} & 1\\ \boldsymbol{1}_{1\times R_h} & \boldsymbol{0}_{1\times R_g} & \boldsymbol{0}_{1\times R_h} & 1\\ -\boldsymbol{\lambda}_h & \boldsymbol{1}_{1\times R_g} & \boldsymbol{\lambda}_h & 0\\ -\boldsymbol{I}_{R_h} & \boldsymbol{0}_{R_h\times R_g} & \boldsymbol{I}_{R_h} & \boldsymbol{0}_{R_h\times 1}\\ \boldsymbol{0}_{R_g\times R_h} & -\boldsymbol{I}_{R_g} & \boldsymbol{0}_{R_g\times R_h} & \boldsymbol{0}_{R_g\times 1}\\ \boldsymbol{0}_{R_h\times R_h} & \boldsymbol{0}_{R_h\times R_g} & -\boldsymbol{I}_{R_h} & \boldsymbol{0}_{R_h\times 1}\end{bmatrix}$$

where $\boldsymbol{1}_{p\times q}$ stands for a $p\times q$ matrix with all ones, $\boldsymbol{\lambda}_h=\eta[\lambda_{h,1},\cdots,\lambda_{h,R_h}]$, and

$$\boldsymbol{m}=-\frac{1}{\ln 2}\left[\frac{\lambda_{h,1}}{\sigma_r^2+\lambda_{h,1}q_1},\cdots,\frac{\lambda_{h,R_h}}{\sigma_r^2+\lambda_{h,R_h}q_{R_h}}\right]$$

$$\boldsymbol{n}=-\frac{1}{\ln 2}\left[\frac{\lambda_{g,1}}{\sigma_d^2+\lambda_{g,1}\lambda_{p,1}},\cdots,\frac{\lambda_{g,R_h}}{\sigma_d^2+\lambda_{g,R_h}\lambda_{p,R_h}}\right].$$

Moreover, $\nabla^2 g_i(\boldsymbol{e}), i = 1, \cdots, 2R_h + R_g + 4$, is the second-order derivative of the ith constraint in (45b), and

$$\sum_{i=1}^{2R_h+R_g+4} \mu_i \nabla^2 g_i(\boldsymbol{e}) = \begin{bmatrix} \mathbf{0}_{R_h\times R_h} & \mathbf{0}_{R_h\times R_g} & \mathbf{0}_{R_h\times R_h} & \mathbf{0}_{R_h\times 1} \\ \mathbf{0}_{R_g\times R_h} & \boldsymbol{J} & \mathbf{0}_{R_g\times R_h} & \mathbf{0}_{R_g\times 1} \\ \mathbf{0}_{R_h\times R_h} & \mathbf{0}_{R_h\times R_g} & \boldsymbol{K} & \mathbf{0}_{R_h\times 1} \\ \mathbf{0}_{1\times R_h} & \mathbf{0}_{1\times R_g} & \mathbf{0}_{1\times R_h} & 0 \end{bmatrix}$$

$$\boldsymbol{J} = \frac{1}{\ln 2}\mathrm{diag}\left(\frac{\mu_2\lambda_{g,i}^2}{(\sigma_d^2+\lambda_{g,i}\lambda_{p,i})^2},\ i=1,\cdots,R_g\right)$$

$$\boldsymbol{K} = \frac{1}{\ln 2}\mathrm{diag}\left(\frac{\mu_1\lambda_{h,i}^2}{(\sigma_r^2+\lambda_{h,i}q_i)^2},\ i=1,\cdots,R_h\right).$$

Finally, $\boldsymbol{r}_d(\boldsymbol{e},\boldsymbol{\mu})$ and $\boldsymbol{r}_c(\boldsymbol{e},\boldsymbol{\mu})$ are the dual residual and the centrality residual, respectively, given by

$$\boldsymbol{r}_d(\boldsymbol{e},\boldsymbol{\mu}) = \nabla g_0(\boldsymbol{e}) + D\boldsymbol{g}(\boldsymbol{e})^T\boldsymbol{\mu} \quad (48)$$

$$\boldsymbol{r}_c(\boldsymbol{e},\boldsymbol{\mu}) = -\mathrm{diag}(\boldsymbol{\mu})\boldsymbol{g}(\boldsymbol{e}) - (1/\omega)\mathbf{1}_{(2R_h+R_g+4)\times 1} \quad (49)$$

where $\nabla g_0(\boldsymbol{e})$ is the first-order derivative matrix of the object function (45a) given by

$$\nabla g_0(\boldsymbol{e}) = [\mathbf{0}_{1\times(2R_h+R_g)},\ 1]^T.$$

REFERENCES

[1] P. Kamalinejad, C. Mahapatra, Z. Sheng, S. Mirabbasi, V. C. M. Leung, and Y. L. Guan, "Wireless energy harvesting for the Internet of Things," *IEEE Commun. Mag.*, vol. 53, no. 6, pp. 102–108, Jun. 2015.

[2] X. Zhou, R. Zhang, and C. K. Ho, "Wireless information and power transfer: Architecture design and rate-energy tradeoff," *IEEE Trans. Commun.*, vol. 61, no. 11, pp. 4754–4767, Nov. 2013.

[3] G. Yang, C. K. Ho, and Y. L. Guan, "Dynamic resource allocation for multiple-antenna wireless power transfer," *IEEE Trans. Signal Process.*, vol. 62, no. 14, pp. 3565–3577, Jul. 2014.

[4] L. R. Varshney, "Transporting information and energy simultaneously," in *Proc. IEEE Int. Symp. Inf. Theory (ISIT)*, Toronto, ON, Canada, Jul. 2008, pp. 1612–1616.

[5] R. Zhang and C. K. Ho, "MIMO broadcasting for simultaneous wireless information and power transfer," *IEEE Trans. Wireless Commun.*, vol. 12, no. 5, pp. 1989–2001, May 2013.

[6] B. Clerckx and E. Bayguzina, "Waveform design for wireless power transfer," *IEEE Trans. Signal Process.*, vol. 64, no. 23, pp. 6313–6328, Dec. 2016.

[7] Y. Zeng, B. Clerckx, and R. Zhang, "Communications and signals design for wireless power transmission," *IEEE Trans. Commun.*, vol. 65, no. 5, pp. 2264–2290, May 2017.

[8] S. H. Chae, C. Jeong, and S. H. Lim, "Simultaneous wireless information and power transfer for Internet of Things sensor networks," *IEEE Internet Things J.*, vol. 5, no. 4, pp. 2829–2843, Aug. 2018.

[9] Q. Shi, L. Liu, W. Xu, and R. Zhang, "Joint transmit beamforming and receive power splitting for MISO SWIPT systems," *IEEE Trans. Wireless Commun.*, vol. 13, no. 6, pp. 3269–3280, Jun. 2014.

[10] G. Yang, C. K. Ho, R. Zhang, and Y. L. Guan, "Throughput optimization for massive MIMO systems powered by wireless energy transfer," *IEEE J. Sel. Areas Commun.*, vol. 33, no. 8, pp. 1640–1650, Aug. 2015.

[11] X. Wang and C. Zhai, "Simultaneous wireless information and power transfer for downlink multi-user massive antenna-array systems," *IEEE Trans. Commun.*, vol. 65, no. 9, pp. 4039–4048, Sep. 2017.

[12] A. A. Nasir, X. Zhou, S. Durrani, and R. A. Kennedy, "Relaying protocols for wireless energy harvesting and information processing," *IEEE Trans. Wireless Commun.*, vol. 12, no. 7, pp. 3622–3636, Jul. 2013.

[13] Z. Ding, S. M. Perlaza, I. Esnaola, and H. V. Poor, "Power allocation strategies in energy harvesting wireless cooperative networks," *IEEE Trans. Wireless Commun.*, vol. 13, no. 2, pp. 846–860, Feb. 2014.

[14] Z. Ding, I. Esnaola, B. Sharif, and H. V. Poor, "Wireless information and power transfer in cooperative networks with spatially random relays," *IEEE Trans. Wireless Commun.*, vol. 13, no. 8, pp. 4400–4453, Aug. 2014.

[15] H. Chen, Y. Li, Y. Jiang, Y. Ma, and B. Vucetic, "Distributed power splitting for SWIPT in relay interference channels using game theory," *IEEE Trans. Wireless Commun.*, vol. 14, no. 1, pp. 410–420, Jan. 2015.

[16] Y. Liu and X. Wang, "Information and energy cooperation in OFDM relaying: Protocols and optimization," *IEEE Trans. Veh. Technol.*, vol. 65, no. 7, pp. 5088–5098, Jul. 2016.

[17] Z. Chu, M. Johnston, and S. L. Goff, "SWIPT for wireless cooperative networks," *Electron. Lett.*, vol. 51, no. 6, pp. 536–538, Jun. 2015.

[18] Z. Ding *et al.*, "Application of smart antenna technologies in simultaneous wireless information and power transfer," *IEEE Commun. Mag.*, vol. 53, no. 4, pp. 86–93, Apr. 2015.

[19] B. K. Chalise, Y. D. Zhang, and M. G. Amin, "Energy harvesting in an OSTBC based non-regenerative MIMO relay system," in *Proc. IEEE ICASSP*, Mar. 2012, pp. 3201–3204.

[20] B. K. Chalise, W.-K. Ma, Y. D. Zhang, H. A. Suraweera, and M. G. Amin, "Optimum performance boundaries of OSTBC based AF-MIMO relay system with energy harvesting receiver," *IEEE Trans. Signal Process.*, vol. 61, no. 17, pp. 4199–4213, Sep. 2013.

[21] G. Amarasuriya, E. G. Larsson, and H. V. Poor, "Wireless information and power transfer in multiway massive MIMO relay networks," *IEEE Trans. Wireless Commun.*, vol. 15, no. 6, pp. 3837–3855, Jun. 2016.

[22] X. Wang, J. Liu, and C. Zhai, "Wireless power transfer-based multi-pair two-way relaying with massive antennas," *IEEE Trans. Wireless Commun.*, vol. 16, no. 11, pp. 7672–7684, Nov. 2017.

[23] C. Zhong, H. A. Suraweera, G. Zheng, I. Krikidis, and Z. Zhang, "Wireless information and power transfer with full duplex relaying," *IEEE Trans. Commun.*, vol. 62, no. 10, pp. 3447–3461, Oct. 2014.

[24] Z. Wen, X. Liu, N. C. Beaulieu, R. Wang, and S. Wang, "Joint source and relay beamforming design for full-duplex MIMO AF relay SWIPT systems," *IEEE Commun. Lett.*, vol. 20, no. 2, pp. 320–323, Feb. 2016.

[25] H. Liu, K. J. Kim, K. S. Kwak, and H. V. Poor, "Power splitting-based SWIPT with decode-and-forward full-duplex relaying," *IEEE Trans. Wireless Commun.*, vol. 15, no. 11, pp. 3837–3855, Nov. 2016.

[26] K. Xiong, P. Fan, C. Zhang, and K. B. Letaief, "Wireless information and energy transfer for two-hop non-regenerative MIMO-OFDM relay networks," *IEEE J. Sel. Areas Commun.*, vol. 33, no. 8, pp. 1595–1611, Aug. 2015.

[27] Y. Huang and B. Clerckx, "Joint wireless information and power transfer for an autonomous multiple antenna relay system," *IEEE Commun. Lett.*, vol. 19, no. 7, pp. 1113–1116, Jul. 2015.

[28] Y. Huang and B. Clerckx, "Relaying strategies for wireless-powered MIMO relay networks," *IEEE Trans. Wireless Commun.*, vol. 15, no. 9, pp. 6033–6047, Sep. 2016.

[29] B. Li and Y. Rong, "AF MIMO relay systems with wireless powered relay node and direct link," *IEEE Trans. Commun.*, vol. 66, no. 4, pp. 1508–1519, Apr. 2018.

[30] B. Li and Y. Rong, "Joint transceiver optimization for wireless information and energy transfer in nonregenerative MIMO relay systems," *IEEE Trans. Veh. Technol.*, vol. 67, no. 9, pp. 8348–8362, Sep. 2018.

[31] A. Antoniou and W.-S. Lu, *Practical Optimization: Algorithms and Engineering Applications*. Spring Street, NY, USA: Springer, 2007.

[32] E. Boshkovska, D. W. K. Ng, N. Zlatanov, and R. Schober, "Practical non-linear energy harvesting model and resource allocation for SWIPT systems," *IEEE Commun. Lett.*, vol. 19, no. 12, pp. 2082–2085, Dec. 2015.

[33] K. Xiong, B. Wang, and K. J. R. Liu, "Rate-energy region of SWIPT for MIMO broadcasting under nonlinear energy harvesting model," *IEEE Trans. Wireless Commun.*, vol. 16, no. 8, pp. 5147–5161, Aug. 2017.

[34] R. Jiang, K. Xiong, P. Fan, Y. Zhang, and Z. Zhong, "Optimal design of SWIPT systems with multiple heterogeneous users under non-linear energy harvesting model," *IEEE Access*, vol. 5, no. 6, pp. 11479–11489, 2017.

[35] K. Choi, D. Kim, and M. Y. Chung, "Received power-based channel estimation for energy beamforming in multiple-antenna RF energy transfer system," *IEEE Trans. Signal Process.*, vol. 65, no. 6, pp. 1461–1476, Mar. 2017.

[36] S. Simoens, O. Munoz-Medina, J. Vidal, and A. del Coso, "On the Gaussian MIMO relay channel with full channel state information," *IEEE Trans. Signal Process.*, vol. 57, no. 9, pp. 3588–3599, Sep. 2009.

[37] K. Xiong, P. Fan, Y. Lu, and K. B. Letaief, "Energy efficiency with proportional rate fairness in multirelay OFDM networks," *IEEE J. Sel. Areas Commun.*, vol. 34, no. 5, pp. 1431–1447, May 2016.

[38] Y. Li, Y. Tian, and C. Yang, "Energy-efficient coordinated beamforming under minimal data rate constraint of each user," *IEEE Trans. Veh. Technol.*, vol. 64, no. 6, pp. 2387–2397, Jun. 2015.
[39] S. P. Boyd and L. Vandenberghe, *Convex Optimization*. Cambridge, U.K.: Cambridge Univ. Press, 2004.
[40] X. Lu, D. Niyato, P. Wang, D. I. Kim, and Z. Han, "Wireless charger networking for mobile devices: Fundamentals, standards, and applications," *IEEE Wireless Commun.*, vol. 22, no. 2, pp. 126–135, Apr. 2015.
[41] S. Pejoski, Z. Hadzi-Velkov, T. Q. Duong, and C. Zhong, "Wireless powered communication networks with non-ideal circuit power consumption," *IEEE Commun. Lett.*, vol. 21, no. 6, pp. 1429–1432, Jun. 2017.

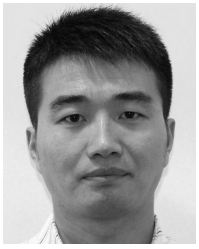

BIN LI (M'18–SM'18) received the bachelor's degree in automation and the master's degree in control science and engineering from the Harbin Institute of Technology, Harbin, China, in 2005 and 2008, respectively, and the Ph.D. degree in mathematics and statistics from Curtin University, Perth, WA, Australia, in 2011. From 2012 to 2014, he was a Research Associate with the School of Electrical, Electronic and Computer Engineering, The University of Western Australia, Perth, WA, Australia. From 2014 to 2017, he was a Research Fellow with the Department of Mathematics and Statistics, Curtin University. He is currently a Research Professor with the School of Electrical Engineering and Information, Sichuan University, Chengdu, China. His research interests include signal processing, wireless communications, optimization, and optimal control.

HANYU CAO received the bachelor's degree in instrument engineering from Sichuan University, where he is currently pursuing the master's degree in control science. His research interests include signal processing, wireless communications, optimization, and optimal control.

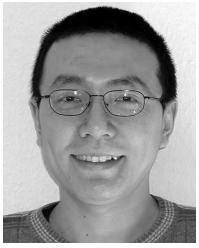

YUE RONG (S'03–M'06–SM'11) received the Ph.D. degree *(summa cum laude)* in electrical engineering from the Darmstadt University of Technology, Darmstadt, Germany, in 2005.

He was a Postdoctoral Researcher with the Department of Electrical Engineering, University of California at Riverside, from 2006 to 2007. Since 2007, he has been with the Department of Electrical and Computer Engineering, Curtin University, Bentley, WA, Australia, where he is currently a Full Professor. His research interests include signal processing for communications, wireless communications, underwater acoustic communications, applications of linear algebra and optimization methods, and statistical and array signal processing. He has published over 160 journal and conference papers in these areas. He was a recipient of the Best Paper Award at the 2011 International Conference on Wireless Communications and Signal Processing, the Best Paper Award at the 2010 Asia–Pacific Conference on Communications, and the Young Researcher of the Year Award of the Faculty of Science and Engineering, Curtin University, in 2010. He was an Editor of the IEEE Wireless Communications Letters, from 2012 to 2014, a Guest Editor of the IEEE Journal on Selected Areas in Communications special issue on theories and methods for advanced wireless relays, and was a TPC Member for the IEEE ICC, IEEE GlobalSIP, EUSIPCO, IEEE ICCC, WCSP, IWCMC, and ChinaCom. He is an Associate Editor of the IEEE Transactions on Signal Processing.

TONGHUA SU received the master's and Ph.D. degrees in computer science from the School of Computer Science and Technology, Harbin Institute of Technology (HIT), in 2003 and 2008, respectively, where he is currently an Associate Professor. He serves as the Director of the HIT-NVidia GPU Research Center and GPU Education Center. He had released the first Chinese handwritten text database, which was used by hundreds of universities and institutes. He initialized the segmentation-free strategy for Chinese handwriting recognition and now evolved as end-to-end strategy. He has published two monographs and translated seven books related to deep learning or GPU computing. His center had been honored as the best GPU education center for four years. His research interests include pattern recognition and GPU computing, especially the deep learning driven agents.

GANG YANG (S'13–M'15) received the B.Eng. and M.Eng. degrees (Hons.) in communication engineering, communication and information systems from the University of Electronic Science and Technology of China, Chengdu, China, in 2008 and 2011, respectively, and the Ph.D. degree from Nanyang Technological University, Singapore, in 2015. In 2015, he was a Research Fellow with the Department of Electrical and Computer Engineering, National University of Singapore. He is currently an Associate Professor with the National Key Laboratory of Science and Technology on Communications, and the Center for Intelligent Networking and Communications (CINC), University of Electronic Science and Technology of China. His current research interests include the Internet-of-Things communications, backscatter communications, wireless powered communications, far-field and near-field wireless power transfer, and compressive sensing. He serves for the IEEE Globecom'17 as the Publicity Co-Chair. He received the Chinese Government Award for Outstanding Self-Financed Students Abroad, in 2015, and the IEEE Communications Society Transmission, Access, and Optical Systems (TAOS) Technical Committee Best Paper Award, in 2016.

ZHIQIANG HE (S'01–M'04) received the B.E. and Ph.D. degrees (Hons.) in signal and information processing from the Beijing University of Posts and Telecommunications, China, in 1999 and 2004, respectively, where he has been with the School of Information and Communication Engineering, since 2004, and is currently a Professor and also the Director of the Center of Information Theory and Technology. He is also a Visiting Scholar with Xiamen University. His research interests include signal and information processing in wireless communications, networking architecture and protocol design, machine learning, and underwater acoustic communications.